Systems biology of bacterial persistence, a metabolism-driven strategy for survival

Radzikowski, Jakub

Chapter 3

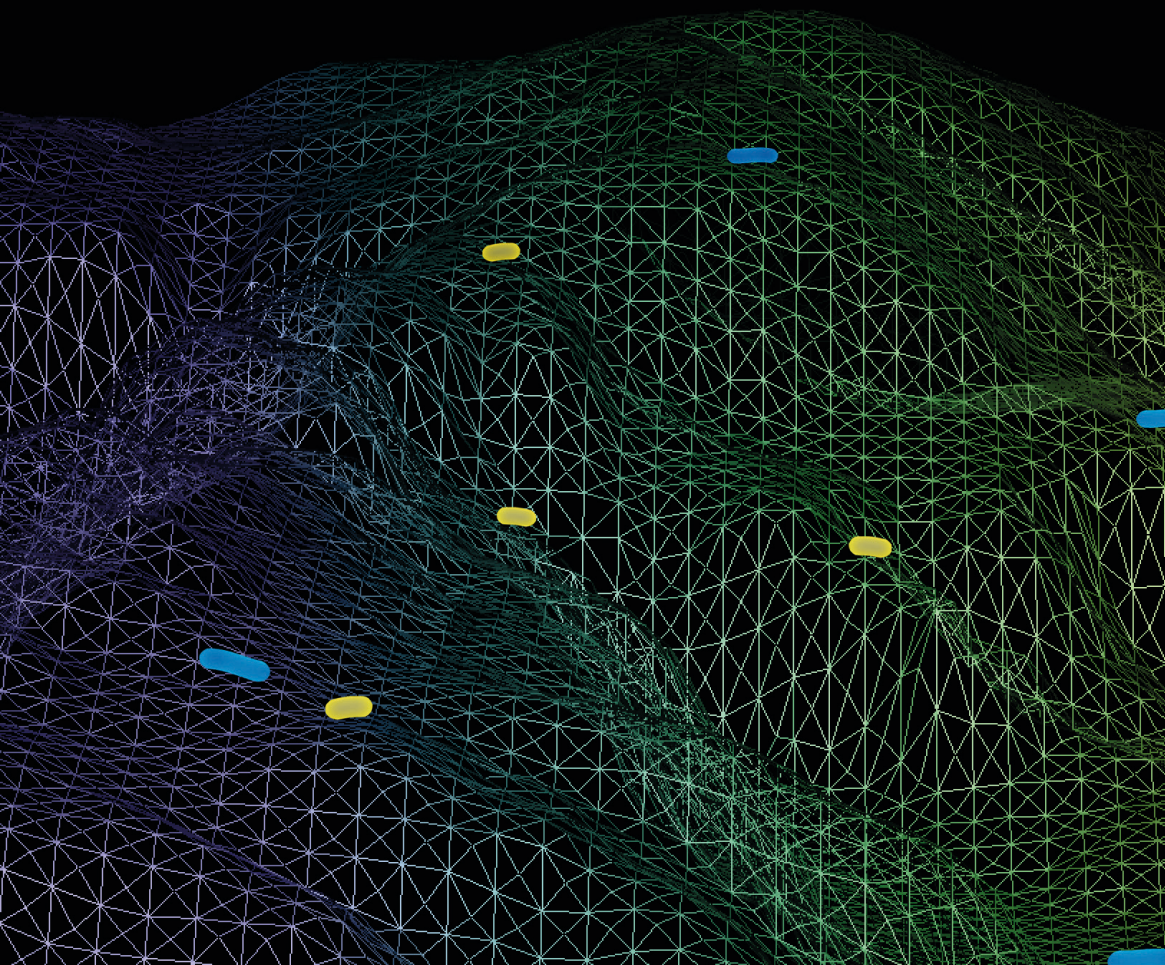

Bacterial persistence is an active σ^S stress response to metabolic flux limitation

Jakub Leszek Radzikowski[1], Silke Vedelaar[1], David Siegel[3], Alvaro Dario Ortega[1], Alexander Schmidt[2] & Matthias Heinemann[1*]

[1]Molecular Systems Biology, Groningen Biomolecular Sciences and Biotechnology Institute, University of Groningen, Nijenborgh 4, 9747AG Groningen, The Netherlands
[2]Biozentrum, University of Basel, Klingelbergstrasse 50/70, 4056 Basel, Switzerland
[3]Analytical Biochemistry Group, Groningen Research Institute of Pharmacy, University of Groningen, Antonius-Deusinglaan 1, 9713AV Groningen, The Netherlands

This chapter is published in Molecular Systems Biology. Radzikowski, J.L., Vedelaar, S., Siegel, D., Ortega, ÁD., Schmidt, A., and Heinemann, M. (2016). Bacterial persistence is an active σ^S stress response to metabolic flux limitation. Mol Syst Biol *12*, 882.

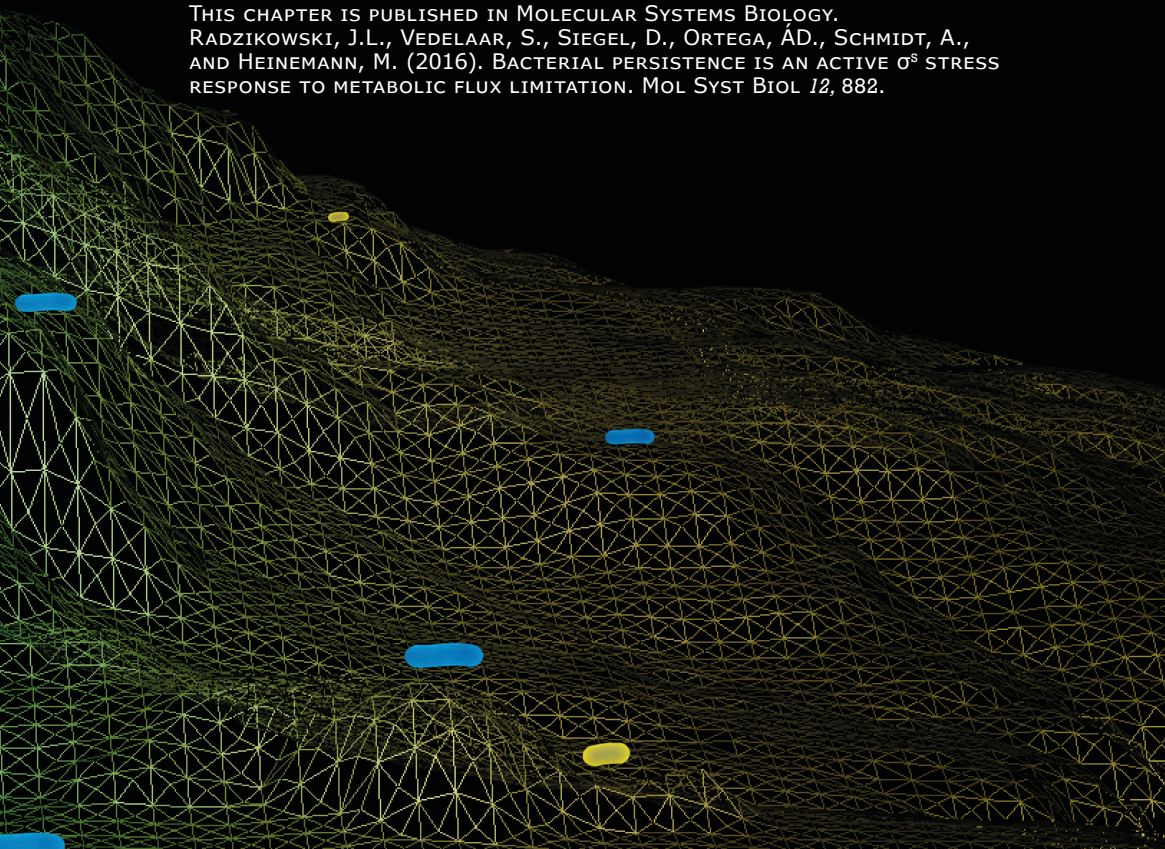

Highlights

- Bacterial persisters are metabolically active, produce energy, and grow.
- The persister proteome is characterized by σ^S–mediated stress response and a shift to catabolism.
- Persistence is an active state that requires a carbon and energy source to be reached.
- Persistence is sustained through a system–level feedback that has low metabolic flux at its core. TAS, σ^S, and elevated ppGpp levels modulate and stabilize this feedback.

Author contributions

JR and MH conceived and designed the study, and wrote the manuscript with input from all authors. JR performed experiments and analyzed the data (antibiotic tolerance with SV, proteomics with AS, metabolite measurements with DS). AO did transcript quantification.

Abstract

While persisters are a health threat due to their transient antibiotic tolerance, little is known about their phenotype and what actually causes persistence. Using a new method for persister generation and high-throughput methods, we comprehensively mapped the molecular phenotype of *E. coli* during the entry and in the state of persistence in nutrient-rich conditions. The persister proteome is characterized by σ^S-mediated stress response and a shift to catabolism; a proteome that starved cells tried to but could not reach due to absence of a carbon and energy source. Metabolism of persisters is geared towards energy production, with depleted metabolite pools. We developed and experimentally verified a model, in which persistence is established through a system-level feedback: strong perturbations of metabolic homeostasis cause metabolic fluxes to collapse, prohibiting adjustments towards restoring homeostasis. This vicious cycle is stabilized and modulated by high ppGpp levels, toxin/anti-toxin systems and the σ^S-mediated stress response. Our system-level model consistently integrates past findings with our new data, thereby providing an important basis for future research on persisters.

Introduction

Bacterial persistence is a phenotypic state of transient antibiotic tolerance that threatens human and animal health (Cohen et al., 2013; Grant and Hung, 2013). This state is typically associated with dormancy in nutrient-rich environments and with absent or low antibiotic target activity, which renders most antibiotics ineffective (Lewis, 2010) and can cause recurrence of infections, with e.g. *Mycobacterium, Staphylococcus* or *Pseudomonas* species (Cohen et al., 2013; Dawson et al., 2011; Fauvart et al., 2011). Despite the importance of persisters, we still have very limited insights into the molecular phenotype of these cells and into what actually triggers persistence.

Bacterial persistence is typically investigated using different *in vitro* models. One persistence model are the antibiotic-tolerant cells that are formed stochastically in growing cultures (Feng et al., 2014; Maisonneuve et al., 2013). Another model for persistence are starved cells (i.e. cells in stationary phase) (Nguyen et al., 2011), which have diminished or absent antibiotic target activity due to the absence of nutrients (Fung et al., 2010). However, it is questionable whether this model is relevant for all types of persisters, as they occur in the host both in the presence (Guarner and Malagelada, 2003; Rohmer et al., 2011) or absence of nutrients (Appelberg, 2006). Finally, a third model for persistence was recently proposed: It was found that after certain nutrient shifts (i.e. abrupt shifts, or gradual

shifts resembling diauxie) a large number of non-/slow-growing and antibiotic-tolerant cells (i.e. persisters) emerge in nutrient-rich conditions (Amato and Brynildsen, 2014; Kotte et al., 2014).

Through isolation of stochastically generated persisters from growing cultures by means of ampicillin treatment or FACS, and through performing transcriptome analyses it was found that - compared to growing cells - persisters have higher abundances of SOS response, cold/hot shock, and toxin/antitoxin systems (TAS) as well as lower levels of flagellum-related transcripts (Keren et al., 2004; Shah et al., 2006). Further, it was found that the fraction of such persister cells could be increased by overexpression of certain toxins such as HipA (Korch and Hill, 2006), RelE (Tashiro et al., 2012), YgiU (Shah et al., 2006) or the Lon protease (Maisonneuve et al., 2011). On the basis of these findings, it was suggested that toxins, higher expressed in individual cells (eventually due to stochastic variation in ppGpp levels) are the decisive factor for persister formation (Maisonneuve et al., 2013). However, neither ppGpp-negative strains (Maisonneuve et al., 2013), rpoS deletion strains (Nguyen et al., 2011), nor strains with multiple TAS deleted (Maisonneuve et al., 2011) were completely free of persisters, suggesting that persister formation can also be achieved through other mechanisms. The involvement of various mechanisms could explain the recently observed heterogeneity between persister cells (Amato and Brynildsen, 2015).

In fact, all three persister models indicate that persister for-

mation could also involve metabolism; next to the involvement of toxin/antitoxin systems. First, the observation that the frequency of stochastically-formed persisters increased with the amount of glucose transport inhibitor added to the growth medium (Maisonneuve et al., 2013) shows that stochastic persister formation depends, at least to some degree, on the magnitude of metabolic flux in single cells. Second, for the nutrient-shift induced persisters, we demonstrated that a limitation in metabolic flux is decisive whether an individual cell adapts to the new nutrient or enters the persister state (Kotte et al., 2014). Finally, in the starvation model, lack of nutrients (and thus lack of metabolic flux) is the cause for the observed persister phenotype. Together, these findings suggest that the metabolic state of a cell and persistence might be closely tethered.

Still, our knowledge about persisters and what exactly triggers their formation is limited. The main problem is that cultures containing only a small fraction of persister cells cannot be subjected to population-averaging experimental methods that require large number of cells. As a matter of fact, the proteome, metabolome, and the physiology (i.e. growth and nutrient uptake) of persister cells are not yet known, as recently highlighted (Amato et al., 2014; Balaban et al., 2013). Here, however, the discovery of the nutrient-shift induced persisters opened up a new possibility to investigate this important bacterial phenotype.

In this work, we exploited the nutrient-shift method to generate large numbers of persisters present in nutrient-rich environ-

ments. First, we demonstrated similarities of these persisters with the stochastically generated ones in terms of antibiotic tolerance, TAS upregulation and ppGpp levels. Then, we determined the phenotype of nutrient-shift-induced and starvation-induced persisters, including the proteome, metabolite levels and physiology of cells during the entry into and in the state of persistence; thereby covering at least two of the currently used persister models. This comparative analysis allowed us to determine the influence of nutrient presence. We found that the metabolism of persisters formed during abrupt glucose to fumarate shift is characterized by low carbon source uptake that sustains a metabolism sufficient for ATP maintenance requirements, and slow growth. Further, we found the proteome of these persisters to be shaped by σ^S, typically associated with starvation and stress. On the basis of our data and previous knowledge, we developed a system-level model on the emergence and sustenance of persisters, which we validated through a series of targeted perturbation experiments. The generated comprehensive description of the persister phenotype and the developed model will form an important basis for future work towards understanding and eradicating persisters.

Results

Following our previous work (Kotte et al., 2014), when we switched *E. coli* cells from glucose to fumarate medium, only an extremely small fraction of cells (0.1% ± 0.05%, SD) adapted and

started to grow on fumarate. The other cells, despite the presence of a utilizable carbon source, entered a state of non-/slow-growth (Kotte et al., 2014), resembling the one of persister cells. Because even 10 to 15 hours after the nutrient shift the growing population reached only 1% of the total population (Supplementary Figure 1A), we could perform population-averaging proteome analyses, metabolite concentration measurements and physiological analyses, with the small fraction of growing cells not significantly influencing the results in the first 8 hours after the shift (cf. Supplementary Text S1). We performed the same analyses on cells that we switched from glucose to medium without a carbon source, generating starved cells, which allowed us to investigate the effect of nutrient presence on the persister phenotype.

Nutrient shifts induce persistence

First, we asked whether the non-/slow-growing cells in nutrient-rich conditions obtained after a nutrient shift and starved cells resemble stochastically-induced persister cells in growing cultures. With the key hallmark of persister cells being transient antibiotic tolerance (Balaban et al., 2013), we specifically asked whether and how fast the cells after the switch to fumarate or to no carbon source become tolerant to antibiotics. Therefore, we treated the cells for 2 h with ampicillin at a concentration that was used for detection of stochastically-formed persisters (Maisonneuve et al., 2011) and that killed fumarate-growing cells, at different time points after the

switch to fumarate medium or medium without a carbon source, and then determined the fraction of surviving cells. In both cases, we found that virtually all cells became tolerant to ampicillin within 30 minutes after the nutrient shift (Figure 1A).

To determine whether the cells also became tolerant against other antibiotics and to identify the dependence of this tolerance on nutrient presence/absence, we exposed the starved cells and the non-/slow growing cells in nutrient-rich conditions (i.e. in presence of fumarate as the carbon source) 4h after the medium shift, to six different antibiotics for 2 h, at concentrations that killed fumarate-growing cells, and determined the fractions of surviving cells. Choosing different antibiotics was motivated by their different mechanisms of action. Observed differences could hint to specific mechanisms increasing antibiotic tolerance between the two tested persister models. Here, we found tolerant cells for all tested antibiotics (Figure 1B). For CCCP (proton gradient disruptor), we found that the non-/slow-growing cells in nutrient-rich conditions survived the antibiotic challenge significantly better (t-test, p-value 0.01) compared to the starved cells. Our results show that non-/slow-growing cells in nutrient-rich conditions and starved cells are tolerant to numerous antibiotics at concentrations that killed fumarate-growing cells. However, the observed difference - namely, the higher tolerance of non-/slow-growing cells in nutrient-rich conditions against CCCP compared to starved cells - suggested that persister cells in nutrient-rich conditions must exploit specific toler-

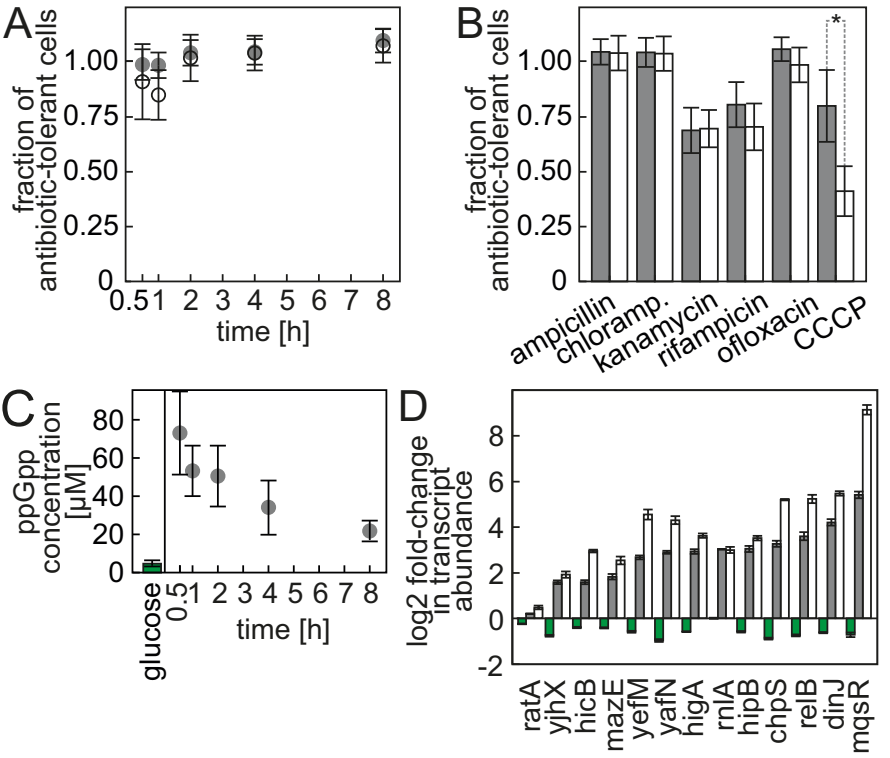
A
fraction of antibiotic-tolerant cells
1.00
0.75
0.50
0.25
0
0.5 1 2 3 4 5 6 7 8
time [h]
B
fraction of antibiotic-tolerant cells
1.00
0.75
0.50
0.25
0
*
ampicillin
chloramp.
kanamycin
rifampicin
ofloxacin
CCCP
C
ppGpp concentration [µM]
80
60
40
20
0
glucose
0.5 1 2 3 4 5 6 7 8
time [h]
D
log2 fold-change in transcript abundance
8
6
4
2
0
-2
ratA
yjhX
hicB
mazE
yefM
yafN
higA
rnlA
hipB
chpS
relB
dinJ
mqsR

Figure 1: Non-/slow-growing cells and starved cells are antibiotic-tolerant, accumulate ppGpp, and express TAS. (A) Dynamics of establishing antibiotic tolerance during entry into non-/slow-growth or starvation. Fraction of antibiotic-tolerant cells after treatment with ampicillin (2 hours, 100 μg mL^{-1}) is shown at various times after the medium switch. Grey disks – non-/slow-growing cells, open circles – starved cells. Data from biological triplicate. Error bars represent one standard deviation. (B) Fractions of antibiotic-tolerant cells after a 2-hour treatment of non-/slow-growing and starved cells with various antibiotics (ampicillin 100 μg mL^{-1}; chloramphenicol 140 μg mL^{-1}; kanamycin 100 μg mL^{-1}; ofloxacin 5 μg mL^{-1}; rifampicin 100 μg mL^{-1}; CCCP 50 μg mL^{-1}) 4h after nutrient switch. Grey bars – non-/slow-growing cells, white bars – starved cells. Data from biological triplicate. Error bars represent one standard deviation. Statistical significance (t-test, or Wilcoxon rank sum test for kanamycin and ofloxacin, p-value < 0.05) is marked with *. (C) ppGpp concentration in cells growing on glucose and in cells shifted from glucose to fumarate medium. Data from biological triplicate. Error bars represent one standard deviation. (D) Log2 fold-change in transcript abundance of first genes in TAS operons compared to cells growing on glucose, normalized to housekeeping gene abundance. Green bars – 2h after switch from glucose medium to glucose medium, grey bars – non-/slow-growing cells 2h after switch from glucose medium to fumarate medium, white bars – starved cells 2h after switch from glucose medium to medium without a carbon source. Data from triplicate experiments. Error bars represent one standard error of the mean.

ance mechanism that enhance their survival over that of persisters generated by starvation.

Elevated levels of ppGpp, occurring for example during amino acid starvation, have been associated with the persister phenotype (Amato et al., 2013; Maisonneuve et al., 2013). To determine whether ppGpp levels are also increased in the non-/slow growing cells obtained after the nutrient shift, we quantified the intracellular ppGpp concentration in these cells, as well as in cells exponentially growing on glucose. Here, we found that ppGpp increases about 16-fold within the first 30 minutes after the shift (t-test p-value = 0.03) and then over the next 7.5 hours decreases to about 5-fold higher levels compared to those on glucose (t-test p-value = 0.03) (Figure 1C).

Another hallmark of stochastically-induced persisters is the involvement of TAS genes (Maisonneuve et al., 2011). To determine whether the non-/slow-growing cells obtained after the nutrient shifts induce transcription of TAS genes, we performed reverse transcription and real-time PCR measurements of 13 different transcripts of the first genes in TAS operons. Here, we found that the shifts to fumarate and to medium without a carbon source both lead to increased abundance of TAS gene transcripts compared to cells growing exponentially on glucose (Figure 1D).

Thus, the nutrient-shift induced persisters have the characteristics of the stochastically-induced persisters: enhanced antibiotic tolerance, increased ppGpp levels, and increased expression of

TAS genes. Remarkably, the slow/non-growing cells in nutrient-rich conditions obtained after a nutrient shift have partly enhanced antibiotic tolerance to CCCP compared to starved cells, suggesting active tolerance mechanisms. In the following, we will call the nutrient-switch induced persisters 'persisters', and the starvation-model persisters 'starved cells'.

Persisters are metabolically active

The enhanced antibiotic tolerance of persisters in nutrient-rich conditions could have been caused by energy availability, which, for instance, could be used to fuel multidrug-efflux systems. To test whether and how the nutrient switch-induced persisters utilize nutrients (i.e. here, fumarate), we determined the physiological parameters of these cells, as well as starved cells and cells normally growing on fumarate. We found that in the first two hours after the switch to fumarate or to medium without a carbon source cells underwent a reductive division characterized by a decrease in cell volume (Figure 2A, Supplementary Table 1) and an increase in cell count (Figure 2B). After that, the persisters grew at a rate of 0.02 ± 0.005 h-1 (95% confidence interval) (Figure 2B) and their volume remained constant (Figure 2A, Supplementary Table 1). As expected, the starved cells did not grow in number (Figure 2B), but they did in volume for the following 6 hours (Figure 2A, Supplementary Table 1). In other bacterial species, such an increase in volume was associated with swelling caused by a lack of membrane poten-

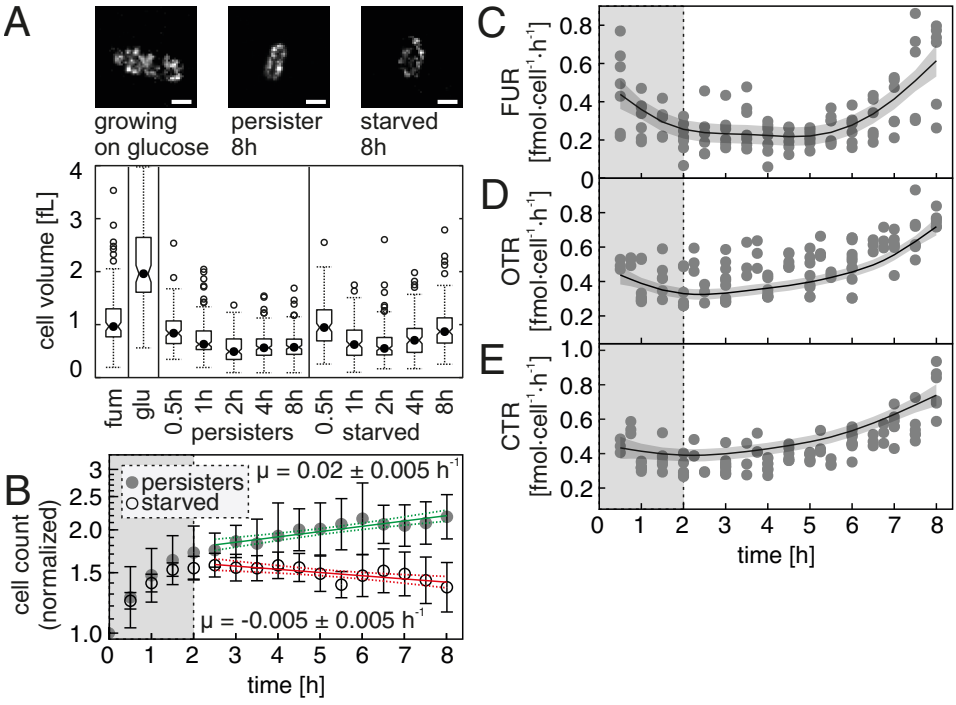
A
growing on glucose
persister 8h
starved 8h
cell volume [fL]
fum
glu
0.5h
1h
2h
4h
8h
persisters
starved
B
persisters
starved
μ = 0.02 ± 0.005 h-1
μ = -0.005 ± 0.005 h-1
cell count (normalized)
time [h]
C
FUR [fmol·cell-1·h-1]
D
OTR [fmol·cell-1·h-1]
E
CTR [fmol·cell-1·h-1]
time [h]

Figure 2: Persisters grow and are metabolically active. (A) Images and cell volumes of cells growing on glucose or fumarate, as well as cells entering persistence and starvation. Scale bars: 1µm. See also Supplementary Table 1. (B) Evaporation-corrected cell count development of cell populations entering persistence and starvation (data from at least 10 replicates). Grey disks – persister cells, open circles – starved cells. Values from each replicate were normalized to t0. Error bars indicate one standard deviation. Green line (persister cells) and red line line (starved cells) represent a prediction of a linear regression fitted to the log-transformed data, where slopes are equal to the growth rate with the dotted lines error margins representing the 95% confidence intervals determined by the model. (C) Time course of the fumarate uptake rate of persister cells. (D) Time course of the oxygen transfer rate (OTR) of persister cells. (E) Time course of the carbon dioxide transfer rate (CTR) of persister cells. Points in C, D and E indicate time-specific rate values, lines indicate fits from generalized additive models with 95% confidence interval (indicated by areas). Vertical grey area in B, C, D and E covering the period from 0 to 2 hours visualizes the period of reductive division. Data from at least three biological replicates.

tial (Rottem et al., 1981). Thus, persister cells, in contrast to starved cells, must have metabolic activity to sustain their slow growth, and possibly to maintain their membrane potential.

Focusing on the nutrient and gas exchange rates in the persister cells, we found that they took up fumarate and oxygen, and produced carbon dioxide, all at rates (per cell) approximately one order of magnitude lower than cells growing on fumarate (Figure 2C-E, Supplementary Table 2). Looking at yields, compared to cells growing on fumarate, persisters produced 5.2 times less biomass per mol of consumed fumarate (Figure 3A), but exchanged more O_2 and CO_2 (2.1 and 1.3 times more per mol of consumed fumarate, respectively; Figure 3B). Thus, the differences between cells growing on fumarate and persisters extend beyond a simple scaling down of the respective metabolic rates. In fact, the higher O_2 and CO_2 yields, in combination with the lower biomass yield in persisters, indicate that persisters respire more, and thus suggest that persisters produce more ATP per mol of consumed carbon source than fumarate-growing cells. We confirmed this conjecture with a flux balance analysis (using a genome-scale model of *E. coli* metabolism (Reed et al., 2003) and the measured physiological rates at 8 hours (Supplementary Table 2) with their 99.5% confidence intervals as constraints and assuming that they represent steady-state conditions as done before (Zampar et al., 2013)), which revealed that the maximum ATP yield (beyond what is needed for biomass production) in persisters is 8.4 times higher than in growing cells

(Figure 3C). Thus, these data indicate that persisters operate their metabolism in a way that is optimized for energy generation, in contrast to biomass production and growth.

Through the flux balance analysis, we also found that persister cells, despite their very low fumarate uptake, could still produce ATP at a maximal rate of approximately 9.5 mmol gDW^{-1} h^{-1} (Figure 3D, note that this is the ATP production rate beyond what is required for growth), a value which is enough to satisfy the non-growth-associated ATP maintenance requirements, which were estimated to between 8 and 10 mmol ATP gDW^{-1} h^{-1} (Orth et al., 2011). Through a metabolome analysis, we found that indeed the adenylate energy charge (AEC = ([ATP] + 0.5 [ADP]) / ([ATP] + [ADP] + [AMP])) was maintained at a high level in persisters (0.74, Figure 3E). The sum of adenylate nucleotide concentrations was identical in persisters and starved cells (Figure 3F), suggesting that the high adenylate energy charge is achieved thanks to energy generation (charging of AMP/ADP with phosphate). In comparison, cells growing on glucose and fumarate had an energy charge of 0.89 and 0.88, respectively (Figure 3E), with values higher than 0.8 being required for growth in *E. coli* (Chapman et al., 1971). In contrast, the adenylate energy charge in starved cells dropped to a value of 0.24 (Figure 3E), as expected from nutrient-deprived cells. Thus, through a metabolism focused on energy generation, persisters in nutrient-rich conditions are able to maintain high energy charges, eventually contributing to the observed enhanced antibiotic tolerance compared to starved cells.

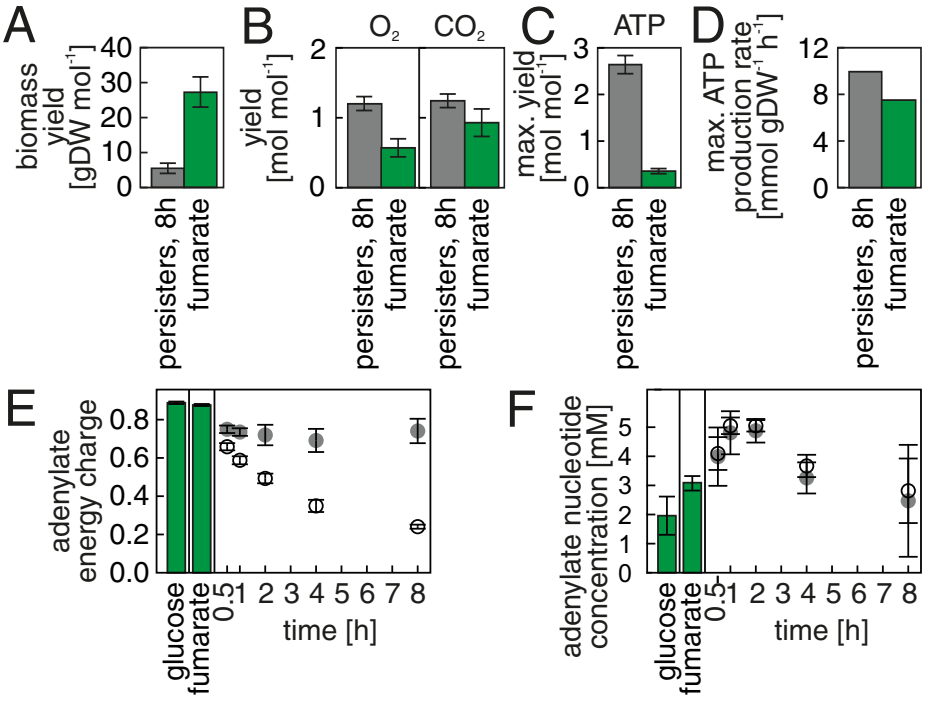
A
biomass yield [gDW mol-1]
40
30
20
10
0
persisters, 8h
fumarate
B
yield [mol mol-1]
2
1
0
O2
CO2
persisters, 8h
fumarate
persisters, 8h
fumarate
C
max. yield [mol mol-1]
3
2
1
0
ATP
persisters, 8h
fumarate
D
max. ATP production rate [mmol gDW-1 h-1]
12
8
4
0
persisters, 8h
fumarate
E
adenylate energy charge
0.8
0.6
0.4
0.2
0.0
glucose
fumarate
0.5 1 2 3 4 5 6 7 8
time [h]
F
adenylate nucleotide concentration [mM]
5
4
3
2
1
0
glucose
fumarate
0.5 1 2 3 4 5 6 7 8
time [h]

Figure 3: Persisters maintain high energy charge levels through respiratory metabolism. (A-C) Persister cells utilize a higher proportion of the taken up carbon for ATP production through respiration and less on biomass formation than cells growing on fumarate. The yields (relative to the up-taken fumarate) were calculated as ratios of physiological rates (cf. Experimental Procedures) and in case of ATP, on the results of the flux balance analysis maximizing ATP production using the estimated physiological rates as constraints. Data from at least three biological replicates. Error bars indicate one standard error of the mean. (D) Maximal possible ATP production rates in persister cells and in fumarate-growing cells, estimated by flux balance analysis maximizing ATP production using the estimated physiological rates as constraints. (E) Adenylate energy charge and (F) sum of adenylate nucleotide concentrations. Grey disks – persister cells, open circles – starved cells, green bars – growing cells. Error bars indicate 95% confidence interval of the mean, calculated with a mixed effects model based on multiple biological replicates in multiple measurement campaigns (cf. Supplementary Table 3).

Persisters achieve a proteome state that starved cells fail to attain

Towards determining the global proteomic phenotype of the persister cells, we next measured levels of about 2000 proteins through liquid chromatography/mass spectrometry proteomics during entry into persistence from glucose (i.e. five time points until eight hours after the shift). For comparison, we measured protein levels in cells growing exponentially on fumarate and glucose, as well as during entry into starvation from glucose or fumarate. The data, i.e. absolute numbers of protein copies per cell, are available online (Radzikowski et al., 2016).

Using the acquired data, we first aimed to identify the global differences between the proteome changes in persister and starved cells. Therefore, we used principal component analyses (PCA) to scale down the almost 2000-dimensional dataset (across 14 different conditions/time points) into a two dimensional PCA space (Figure 4, upper and middle panels). Here, we found that with time the persisters' proteome increasingly deviated from the proteome of glucose-grown cells (Figure 4A). Interestingly, although all cells were switched to fumarate, the proteome of persister cells did not approach the one of fumarate-growing cells. In fact, the proteomes of fumarate- and glucose-growing cells were more similar to each other than the proteome of persister cells compared to either the proteome of glucose-growing cells or fumarate-growing cells

(Pearson's r = 0.86, 0.75 and 0.66, respectively).

Furthermore, we found that the changes in the proteome of starved cells, which almost exclusively occurred during the first two hours after the nutrient shift, followed the same trajectory as the proteome changes in the persister cells (Figure 4B). However, likely due to the lack of a carbon and energy source, the proteome of starved cells did not reach the same state as persister cells. Remarkably, the proteome of starved cells, which were previously grown on fumarate, also moved in the same direction as the proteomes of persisters and of starved cells generated from glucose-growing cells (Figure 4B). These findings implied that the proteome adjustments in both starved and persister cells must be caused by a common cue, which is not specific to the availability of a carbon source in the medium.

Persister proteome is characterized by enhanced catabolism and σ^S-driven stress response

One factor inherent to the proteome changes of persister and starved cells is the downshift in growth rate (Figure 2B). Growth rate affects gene expression (Klumpp et al., 2009) and was identified to be a major factor in reorganizing proteome upon gradual glucose exhaustion (Berthoumieux et al., 2013). Thus, the observed proteome changes in the persister cells could be a simple consequence of the decrease in growth rate. To decipher whether the

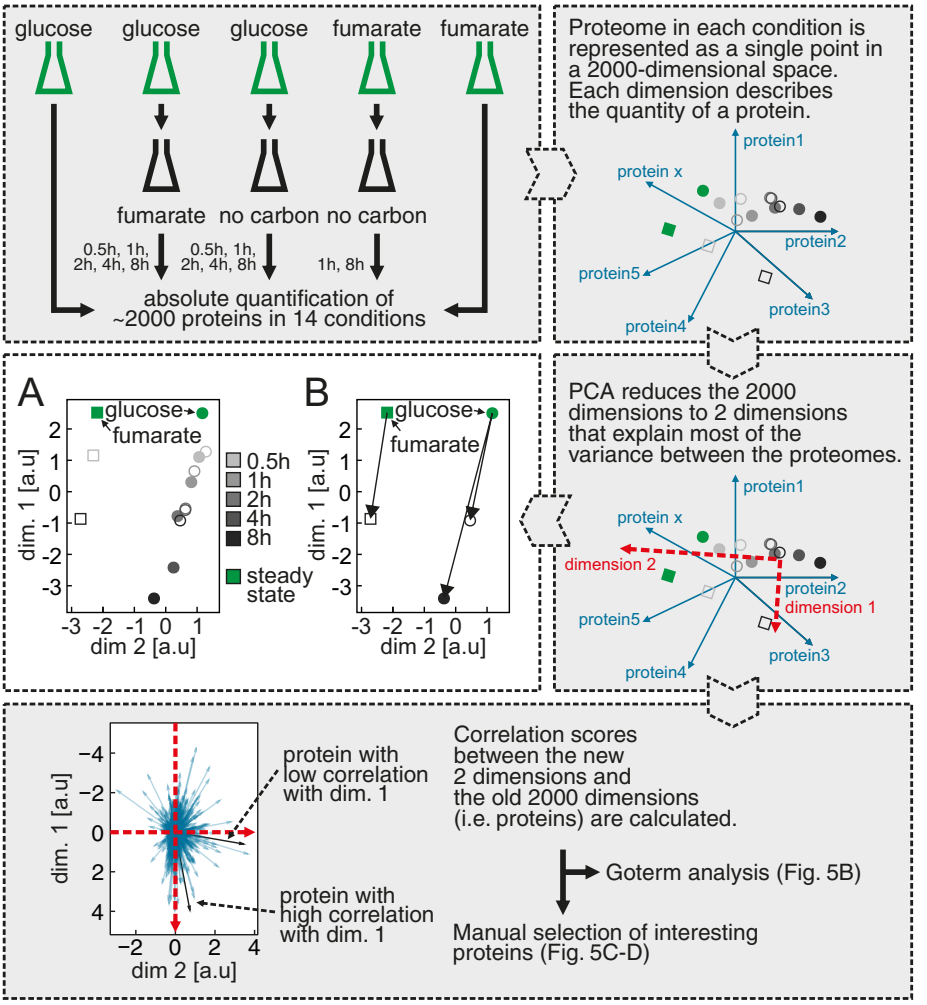
glucose
glucose
glucose
fumarate
fumarate
fumarate
no carbon
no carbon
0.5h, 1h, 2h, 4h, 8h
0.5h, 1h, 2h, 4h, 8h
1h, 8h
absolute quantification of ~2000 proteins in 14 conditions
Proteome in each condition is represented as a single point in a 2000-dimensional space. Each dimension describes the quantity of a protein.
protein1
protein x
protein2
protein5
protein3
protein4
A
B
glucose
fumarate
dim. 1 [a.u]
dim 2 [a.u]
0.5h
1h
2h
4h
8h
steady state
PCA reduces the 2000 dimensions to 2 dimensions that explain most of the variance between the proteomes.
dimension 2
dimension 1
protein with low correlation with dim. 1
protein with high correlation with dim. 1
Correlation scores between the new 2 dimensions and the old 2000 dimensions (i.e. proteins) are calculated.
Goterm analysis (Fig. 5B)
Manual selection of interesting proteins (Fig. 5C-D)

Figure 4: Persisters' and starved cells' proteome are shaped by the same cue. The experimental and data analysis procedure is described in the grey boxes step by step. (A) PCA plot of the *E. coli* proteomes in different conditions and time points. Each point represents a proteome in a different state. The distances between points are inversely correlated with the similarity between proteomes (i.e. proteomes with higher correlation coefficient have a shorter distance between each other), calculated based on differences in the expression level of each quantified protein. Green disk – cells growing on glucose, green square – cells growing on fumarate, grey disks – cells entering persistence after glucose to fumarate switch, open circles – cells entering starvation from glucose, open squares – cells entering starvation from fumarate. Time series are indicated by grey color gradients. (B) The progression of changes upon entry into starvation and entry into persistence happens in the same direction in the 2-dimensional space, indicating that the same cue shapes these proteomes.

observed changes are a mere reflection of growth rate changes or whether the observed changes resemble specific characteristics of persisters, we made use of the proteome data that we recently generated when *E. coli* was grown on 11 different carbon sources and under 3 different stress conditions (Schmidt et al., 2016). We projected these proteomes onto the PCA space created by the proteomes of this study (see above). Here, we found that the proteomes of cells growing on different carbon sources, and thus at different growth rates, were mainly distributed along the dimension 2 of the PCA space, while the proteomes of the cells grown under the stress conditions moved along the dimension 1, as did the proteomes of persister cells and starved cells measured in this study (Figure 5A). The fact that persister cells and starved cells moved along the same direction as the stressed cells (i.e. pH, temperature and osmotically stressed cells) suggests that a general stress response, or the stringent response triggered by the increased ppGpp levels (Figure 1C), is the driving force behind the specific proteome adjustments in persister and starved cells, instead of a global growth rate effect.

We next sought to identify the specific characteristics of the persister proteome. Therefore, we again used PCA together with a GOterm enrichment analysis, this time comparing persister cells at 8 hours with the proteomes of growing cells, and separately with starved cells at 8h (Figure 4, lower panel). In the first analysis, for which the results are shown in Figure 5B, we found that the proteins of 'dimension 1' explain 75.2% of the total variation between the

data of persister cells and growing cells. The enrichment analysis of this separating dimension showed that the persister proteome, compared to growing cells' proteomes, was characterized by lower levels of proteins for DNA replication, recombination and SOS response (Figure 5B, see Supplementary Table 4 for full ranked list). On the other hand, persister cells had higher levels of proteins responsible for stress response, including response to starvation, RNA catabolism, DNA repair as well as protein folding (e.g. chaperones). In persisters, also a shift towards catabolism was observed (i.e. lower abundances of proteins for nucleotide, amino acid and cofactor biosynthesis and higher abundance of glycolysis proteins) (Figure 5B). When comparing persisters and starved cells, the analysis revealed similar processes to be up-regulated as between persisters and growing cells (Figure 5B). This finding indicated - consistent with the analysis shown in Figure 4A - that the differences between the starved and the persister proteome lie mostly in the *strength* of protein expression changes and not in the *kinds* of proteins being expressed. Overall, the proteome of persisters (and to a lesser extent also the one of starved cells) was mostly characterized by a shift towards catabolism, as well as global stress response, compared to exponentially growing cells.

To identify proteins that particularly contribute to the observed phenotype of persister cells, we looked for proteins that were most significantly correlated with the separating 'dimension 1' (which characterizes the persister-specific differences). One of

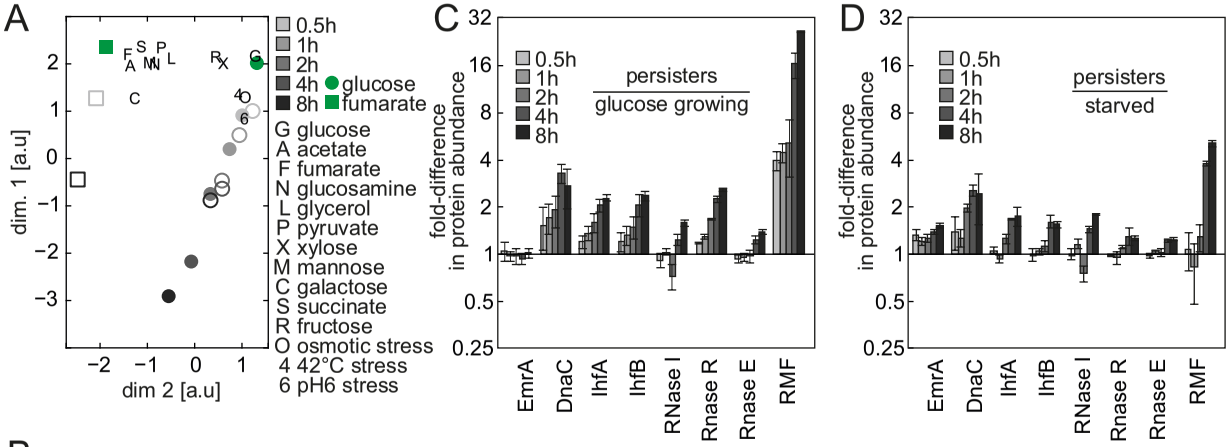
A
dim. 1 [a.u]
dim 2 [a.u]
0.5h
1h
2h
4h glucose
8h fumarate
G glucose
A acetate
F fumarate
N glucosamine
L glycerol
P pyruvate
X xylose
M mannose
C galactose
S succinate
R fructose
O osmotic stress
4 42°C stress
6 pH6 stress
C
fold-difference in protein abundance
persisters / glucose growing
D
persisters / starved
EmrA
DnaC
IhfA
IhfB
RNase I
Rnase R
Rnase E
RMF

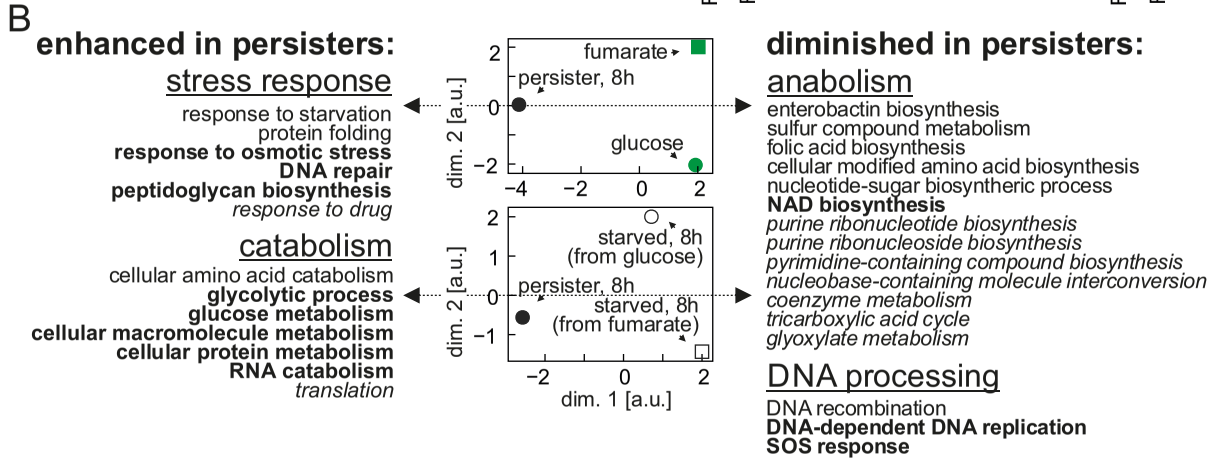
B
enhanced in persisters:
stress response
response to starvation
protein folding
response to osmotic stress
DNA repair
peptidoglycan biosynthesis
response to drug
catabolism
cellular amino acid catabolism
glycolytic process
glucose metabolism
cellular macromolecule metabolism
cellular protein metabolism
RNA catabolism
translation
fumarate
persister, 8h
glucose
starved, 8h (from glucose)
persister, 8h
starved, 8h (from fumarate)
dim. 2 [a.u.]
dim. 1 [a.u.]
diminished in persisters:
anabolism
enterobactin biosynthesis
sulfur compound metabolism
folic acid biosynthesis
cellular modified amino acid biosynthesis
nucleotide-sugar biosyntheric process
NAD biosynthesis
purine ribonucleotide biosynthesis
purine ribonucleoside biosynthesis
pyrimidine-containing compound biosynthesis
nucleobase-containing molecule interconversion
coenzyme metabolism
tricarboxylic acid cycle
glyoxylate metabolism
DNA processing
DNA recombination
DNA-dependent DNA replication
SOS response

Figure 5: Proteome of persisters has enhanced catabolism and activation of stress response. (A) Projection of E.coli proteomes in various growth and stress conditions (Schmidt et al., 2016) on the PCA space created by proteomes generated in this study. (B) PCA of proteomes of persister, fumarate-growing and glucose-growing cells (upper panel); PCA of proteomes of persister cells and starved cells that were growing on glucose or fumarate before starvation (lower panel), markers as in A. GOterms shared between the two analyses (i.e. persisters vs. growing cells and persisters vs. starved cells) are indicated in bold. GOterms specific to persisters vs. starved cells analysis are indicated in italics. For a ranked list of assigned GOterms, see Supplementary Table 4. See also Supplementary Figure 2 showing expression levels of proteins involved in E. coli central metabolic pathways. (C-D) Time profiles of abundance of selected proteins that are significantly correlated with the persister phenotype in both PCA analyses (i.e. proteins for which the correlation coefficient had $p<0.1$). Abundance relative to cells growing on glucose (C) or relative to starved cells (D). Error bars indicate one standard deviation reflecting variation between technical replicates.

these proteins (Figure 5C-D) is EmrA, a protein involved in CCCP export and resistance to this drug (Lewis et al., 1994), which had a 1.6-fold higher concentration in persisters than in starved cells, eventually explaining the higher tolerance of persisters to this drug (cf. Figure 1B). Other notable differences included proteins involved in DNA replication, transcription and translation. As for replication, we found higher levels of IHF (integration host factor) in persisters compared to both growing and starved cells (IhfA - 2.3 and 1.7 fold; IhfB – 2.4 and 1.6 fold, respectively). As the integration host factor has been found to enhance initiation of replication (Friedman, 1988), its higher abundance might point to an enhanced capability to initiate replication in persister cells, which would prime them for resuming growth. We also found higher levels of DnaC in persisters compared to cells growing on glucose (2.8-fold). DnaC was found to be crucial for restarting stalled replication forks (Nusslein-Crystalla et al., 1982), and required for initiation of replication (Kaguni et al., 1985). If indeed the higher levels of these proteins enhance the persisters cells' ability to replicate DNA, then potentially, persisters are ready to resume replication and growth.

As for translation, we found proteins involved in post-transcriptional regulation to be increased in persisters, compared to growing cells. Specifically, we observed higher levels of ribonucleases in persisters: RNase I (*rna,* 1.6 fold), R (*rnr,* 2.6 fold), and E (*rne* 1.4 fold). While the two first RNases are responsible for rRNA degradation (Cheng and Deutscher, 2002; Kaplan and Apirion, 1974),

RNase R and RNase E are also responsible for mRNA degradation, the latter being also involved in specifically degrading transcripts essential for growth (i.e. ftsA-ftsZ) (Cam et al., 1996; Cheng and Deutscher, 2005). The persister proteome is also characterized by higher levels of RMF (ribosome modulation factor, 26.4-fold), which was found to cause the dimerization of the 70S ribosomes, also in persisters (Cho et al., 2015), leading to global inhibition of translation. These results suggest that in persisters the cellular processes of transcription and translation might be inhibited by mechanisms extending beyond toxin-antitoxin systems. The generally stronger overexpression of the above-mentioned proteins in persisters compared to starved cells again indicates that the main difference between the proteomes of persister cells and starved cells is caused by availability of nutrients and the rudimentary metabolic activity of persisters.

Next, we aimed to identify the regulatory factors responsible for the proteome of persisters. Here, σ^S and the stress response was a good candidate, as the comparative analysis above suggested a stress response to be specific for the persister proteome. This notion was also in agreement with the fact that a lack of σ^S affected the frequency of persister cell formation (Nguyen et al., 2011) and that σ^S levels were increased in stochastically-formed persister cells (Maisonneuve et al., 2013). Indeed, we found the levels of σ^S to be increased upon entry into persistence (5.5-fold difference compared to glucose-growing cells) as well as into starvation (3.9-fold differ-

ence compared to glucose-growing cells) and were maintained at about 1.5 times higher level in persister cells compared to starved cells 8 hours after the medium switch (Supplementary Table 5).

However, because mRNA of σ^S-induced genes could be subject to post-transcriptional regulation, just from the higher abundance of this sigma factor we could not yet conclude that σ^S is truly responsible for the shape of the persister proteome. However, when focusing on the genes regulated by σ^S (Salgado et al., 2013), for which we had protein concentrations measured, we found that 67 out of 174 proteins were more than 2-fold overexpressed and only 11 out of 174 were more than 2-fold depleted in persisters compared to glucose growing cells. In starved cells, we found 41 out of 174 proteins to be more than 2-fold overexpressed and 11 out of 174 to be more than 2-fold depleted compared to glucose growing cells (Supplementary Table 6).

To establish that the changes in persister proteome were indeed governed by σ^S, we performed a hypergeometric test using known sigma factor-gene interactions, transcription factor (TF)-gene interactions and regulatory RNA-gene interactions (all from the RegulonDB database; (Salgado et al., 2013)) on genes with at least 2-fold change in protein abundance, selected by clustering along similar profiles of protein concentration change in time with STEM software. Here, we found that in persister cells σ^S had the lowest p-value of all regulatory factors (FDR-adjusted $p = 0.015$; all other sigma factors and TF factors as well as regulatory RNA the p-val-

ues were higher than 0.05). This finding indicated that the proteome changes in persister cells were largely controlled by σ^S.

Consistent with the general function of stress response to limit the demand for resources and to ensure survival (Hardiman et al., 2007; Shimizu, 2013), our PCA analysis did not reveal any changes in the persisters' metabolic proteome towards adapting these cells to the new condition (i.e. growth on fumarate in this case). The revealed up-regulation of glycolytic proteins (less-than-2-fold compared to glucose-growing cells, Figure 5B, Supplementary Figure 2) is not needed for growth on fumarate, as it is a gluconeogenic substrate. In fact, the only major differences we found in central metabolic enzymes between persister and growing cells (i.e. the fumarate reductases and the aconitase) can be explained by the regulatory action of σ^S.

Overall, we found that σ^S is primarily responsible for the proteome of persisters. Because we also found that σ^S is up-regulated in starved cells (Supplementary Table 5), the cue for entering the persister state in nutrient-rich conditions must be the same as for entering starvation. As σ^S was up-regulated for the whole period of our observation in persisters and starved cells (Supplementary Table 5), this suggests that the cue inducing the σ^S stress response must be sustained over time. Because persisters maintain metabolic activity, change protein expression and grow, it is interesting to ask what is the cue, or the factor, which causes them to perceive starvation even though nutrients are available. Increased ppGpp

levels cause an up-regulation of σ^S expression (Gentry et al., 1993). As we found elevated ppGpp levels in persisters (Figure 1C), these increased ppGpp concentrations could be the cause for the higher abundance of σ^S in persister cells. However, it is still a question which mechanism would cause ppGpp levels to be increased in persisters, and what is the cue triggering this mechanism.

Persister cells and starved cells share a distinct metabolite pool pattern

While the proteome of both persisters and starved cells was triggered in response to likely the same cue, our physiological characterization demonstrated that this signal cannot be the cells' energetic state, or a lack of metabolic activity, because these two features were strongly different in persisters and starved cells. However, intracellular metabolite concentrations, which can regulate gene expression (cf. (Kochanowski et al., 2013)), could serve as the signal triggering the stress response in persister cells present in nutrient-rich conditions as well as in starved cells. In search for such a metabolic cue, we measured the concentrations of 29 metabolites of central carbon metabolism as well as of energy and redox cofactors at different time points during entry into persistence and starvation, and in cells growing exponentially on fumarate and on glucose.

Here, we found that compared to growth on glucose and fu-

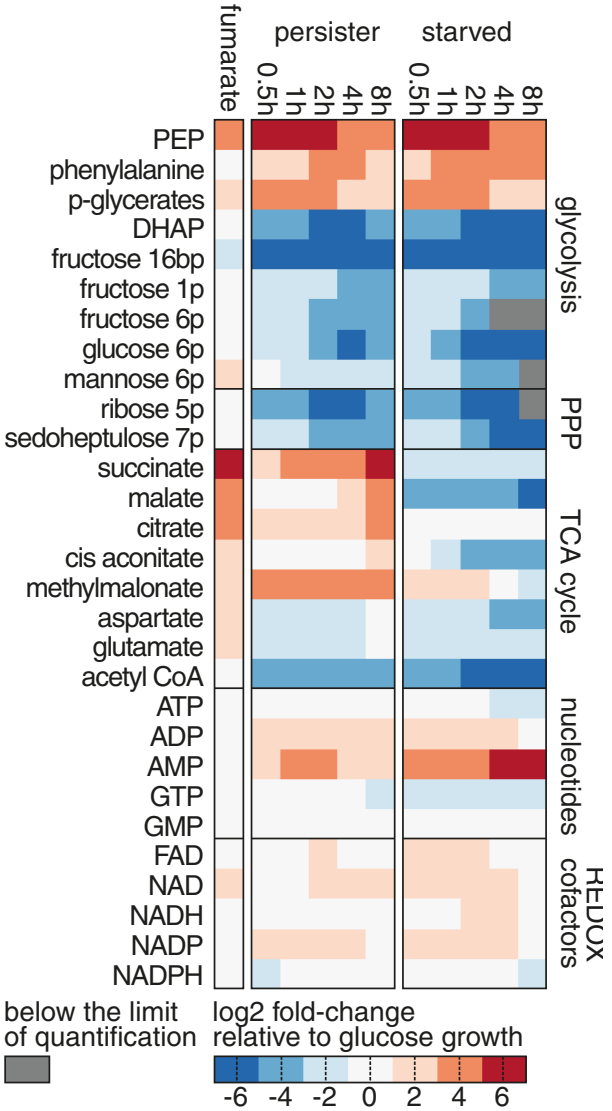

Figure 6: Persister and starved cells have depleted metabolite pools. Change in metabolite concentrations in persister, starved and fumarate-growing cells relative to glucose-growing cells. For absolute concentrations with error estimates and numbers of replicates, see Supplementary Table 3.

marate, the concentrations of most glycolytic and pentose phosphate pathway intermediates dropped one to two orders of magnitude to concentrations in the μM range in the first 30 minutes of entry into persistence and starvation (Figure 6). The only glycolytic metabolites with higher concentrations in persisters and starved cells, compared to glucose-grown cells, were phosphoenolpyruvate (PEP) and the PEP derivatives, phosphoglycerates and phenylalanine. The tricarboxylic acid cycle intermediates, most probably due to fumarate as the chosen carbon source, had higher concentrations in persisters compared to the starved cells; as high as in fumarate-growing cells. The distinct concentration pattern of glycolytic metabolites (i.e. extremely low levels with the exception of increased levels of PEP and phosphoglycerates), similar in starved cells and persister cells, could contain the signal for the entry and sustenance of the stress response.

Low metabolic flux causes persister formation without σ^S or TAS action

On the basis of our generated data and previous persister cell studies, we developed a conceptual model for the entry into and the sustenance of the persister state (Figure 7A). At the core of this model is a positive feedback loop that can drive cells into and arrest them in the persister state. According to this model, a trigger for entry into persistence are strong perturbations of metabolic homeostasis - perturbations beyond the intrinsic buffering capac-

ities of enzymes or beyond possible adjustments of enzyme levels - leading to critically lowered metabolic fluxes. At such low fluxes, a correction of metabolism is impossible, because rates of protein synthesis could be lower than the rates of protein degradation. As such, at critically low metabolic fluxes it might be impossible for cells to restart metabolism or to re-adjust metabolic homeostasis. Together, these mechanisms could form a sort of vicious cycle (i.e. feedback) leading to persistence (Figure 7A). It should be noted that this proposed feedback mechanism does not involve toxins and is therefore different to the one proposed by (Klumpp et al., 2009), who suggested a toxin-based feedback mechanism resulting in growth-bistability during steady-state growth.

Our model further suggests that the robustness of such 'low-level' vicious cycle could be enhanced by the stress response and toxin/antitoxin systems, as well as other inhibitory mechanisms such as RMF-induced ribosome dimerization. These mechanisms could strengthen the feedback by inhibiting translation, transcription and replication, or by allocating the limiting resources (under the perturbation of metabolic homeostasis) to stress response. Such allocation of resources would further reduce (or prevent) metabolic adjustments or corrections, although with the resources still available it might also be possible to attempt restoring metabolic homeostasis. These feedback-enhancing mechanisms would likely ensure bacterial survival during strong perturbations of metabolic homeostasis, by prohibiting that cells engage in 'risky' metabolic

A
induced or stochastic restoration of metabolic homeostasis
induced or stochastic perturbation of metabolic homeostasis
low metabolic flux
SpoT
ppGpp
stringent response
TAS
inhibition of transcription, translation, & replication
active restoration of homeostasis by metabolic adaptation
B
fraction of growing cells
BW25113
Δrmf
ΔrelA
ΔrpoS
MG1655
Δ10
Δ10ΔrpoS
C
RpoS overexpression BW25113 ΔrpoS
fraction of growing cells
0 IPTG
[IPTG] [uM]
D
DctA overexpression MG1655 Δ10ΔrpoS
fraction of growing cells
0 IPTG
[IPTG] [uM]
E
2gL-1 fumarate
+1gL-1 glu
forward scatter (normalized)
cell count (normalized)
time [h]

Figure 7: Persistence is sustained through a system-level feedback loop. (A) A metabolic perturbation beyond the intrinsic buffering capacity of metabolism, which results in low metabolic flux, is the trigger for persistence. Cells with such low metabolic flux cannot not restore metabolic homeostasis, creating feedback and thus a vicious cycle. The robustness of this primitive, system-level feedback loop can be enhanced via various mechanisms, such as action of TAS, σ^S or ppGpp, which lead to further inhibition of transcription and translation. The system-level feedback loop is active until the vicious cycle is broken through restoration of metabolic homeostasis, for example, by addition of certain nutrients, stochastically higher expression of certain flux-limiting enzymes or stochastically low expression of growth inhibiting mechanisms. (B) Fraction of growing cells (i.e. 1 – fraction of persister cells) in various knock-out strains after a glucose to fumarate nutrient shift. White bars – BW25113-derived strains. Grey bars – MG1655-derived strains. Δ10 – strain with 10 TAS knocked-out. Statistically significant difference (t-test, or Wilcoxon rank sum test for Δrmf, p-value < 0.05) between the mutants and the respective wildtype is indicated with an asterisk (*). Mean of at least 3 replicates and standard deviations are shown. See Supplementary Table 7 for antibiotic tolerance assay results. (C) Fraction of growing cells after a glucose to fumarate shift decreases with higher induction of σ^S expression in ΔrpoS strain. Cells were induced with IPTG at the indicated concentrations after the nutrient shift. (D) Fraction of growing cells after a glucose to fumarate shift increases with higher induction of DctA fumarate transporter, and thus with higher metabolic flux, in the Δ10ΔrpoS strain. Cells were induced with the indicated IPTG concentrations for 16 hours prior to the nutrient shift and after the nutrient shift. Mean of 3 replicates and standard deviations are shown. (E) Rapid increase in forward scatter and cell count upon addition of glucose (at 4 hours after nutrient shift) indicates that persister cells can rapidly resume growth upon externally driven restoration of metabolic homeostasis. Forward scatter distribution from 3 replicates, and cell count mean of 3 replicates and standard deviations are shown.

adjustments and instead invest in stress response and maintenance given the available limited resources (indicated by low metabolic fluxes).

On the basis of the identified characteristic metabolite pool pattern, we hypothesize that activation of the observed stress response could occur through a metabolite, which modulates the activity of (or being one of the substrates for) the ppGpp synthases RelA or SpoT leading to increased levels of ppGpp to trigger the stringent and other stress responses. According to our model, perturbations in components such as the TAS, σ^S, or ppGpp synthesis should either sensitize or de-sensitize the feedback loop depending on the nature of the perturbation, but not abolish the feedback loop between low metabolic fluxes and lack of metabolic adjustment/correction. Thus, TAS, σ^S, or ppGpp synthase perturbations should only modulate the fraction of persister cells, but not eliminate them.

To test whether the currently known growth-inhibiting persistence mechanisms, TAS and RMF, indeed only modulate the fraction of persister cells, we switched various mutant strains from glucose to fumarate and assessed the number of persisters emerging: We tested Δrmf (ribosome modulation factor, inhibitor of protein synthesis) in our wild type background (BW25113), as well as the 10 TAS knock out strain generated in Kenn Gerdes' lab (Δ10, (Maisonneuve et al., 2011)) and the respective parental strain, MG1655. Here, we found that deleting neither the TAS systems nor the ribosome

modulation factor changed the fraction of cells adapting to fumarate (Figure 7B) and thus the fractions of persisters formed. Next, we investigated the role of σ^S and stress response, which, on the basis of our proteome analyses, we speculated to have a significant role in establishing the persister phenotype. First, consistent with the fact that the ppGpp synthase RelA is primarily involved in amino acid starvation response (Haseltine and Block, 1973), we found that its deletion did not modulate the fraction of adapting cells and thus not the amount of persisters formed (Figure 7B). This finding suggests that here rather SpoT (the second *E. coli* ppGpp synthase) might be responsible for synthesizing ppGpp, and for its increased concentration (Figure 1C). As a deletion of *spoT* was never achieved without obtaining spontaneous suppressor mutations in the *relA* gene (Montero et al., 2014), and the double knock-out strain Δ*relA*Δ*spoT* cannot grow without certain amino acids (Xiao et al., 1991), we directly tested the Δ*rpoS* strain (*rpoS* encodes for σ^S). Deleting *rpoS* in the BW25113 background and in the Δ10 strain both significantly increased the number of cells adapting to fumarate (t-test p-value = 0.0025 and 0.0032, respectively) (Figure 7B) and thus decreased the number of persisters. To perturb the system in the opposite direction, we complemented the BW25113 Δ*rpoS* strain with a plasmid for IPTG-inducible expression of σ^S and switched the cells from glucose to fumarate medium supplemented with different IPTG concentrations. Here, we found that with progressively higher concentrations of IPTG (and thus higher σ^S expression levels) more cells

assumed the persister phenotype (Figure 7C). These findings show that σ^S modulates the strength of the feedback and thus the amount of persisters, most probably as a response to SpoT activity. However, persisters also occurred in absence of σ^S (Figure 7B). Therefore, also σ^S is not essential, but still plays a role in establishing the persister state.

Because the growth-inhibiting mechanisms currently thought to be responsible for persister formation did not lead to complete elimination of persister cells, these findings provide further evidence towards the proposed metabolic flux-dependent primitive vicious cycle forcing cells into persistence (Figure 7A). Critical perturbations of metabolic homeostasis leading to lowered metabolic fluxes could be low expression (for instance, for stochastic reasons) of flux-controlling enzymes or nutrient transporters (Kiviet et al., 2014), drastic nutrient shifts, reductions of nutrient influx, or complete nutrient-deprivation (for instance, during stationary phase). In fact, it has been shown that the fraction of persisters inversely correlated with glucose influx (Maisonneuve et al., 2013), and with acetate or fumarate influx (Kotte et al., 2014). To test whether the entry into persistence is still metabolic-flux-dependent in a strain that lacks TAS and σ^S, which would provide further support for the primitive vicious cycle, we transformed the Δ10 Δ*rpoS* strain with a plasmid for IPTG-inducible expression of the fumarate transporter DctA, through which we could previously modulate the metabolic flux upon shifts to fumarate (Kotte et al., 2014). Here, we found that

with increasing DctA expression and thus increasing fumarate uptake flux, the fraction of persisters indeed decreased (Figure 7D). This finding, together with the fact that the Δ10 TAS Δ*rpoS* strain still produced persisters upon a nutrient shift (Figure 7B), provided further support to our model, in which the metabolic flux is the basic factor in establishing persistence, while other mechanisms enhance the feedback.

Finally, according to our model, a change to beneficial environmental conditions should immediately break the vicious cycle by enabling persister cells to regain homeostasis passively without adjustment of the metabolic machinery. To test whether this is indeed the case, we added glucose to the persister cells 4 hours after the shift to fumarate. We found that the cells indeed started growing in size (measured via forward scatter) and in number, virtually immediately after the addition of glucose (Figure 7E). This finding suggests that the factors inhibiting persister growth can be removed on a very short time scale.

Discussion

Using a recently proposed way to generate persisters in large quantities, and high-throughput analytical methods, we comprehensively mapped the molecular phenotype of cells during the entry and in the state of persistence in nutrient-rich conditions. We found that *E. coli* persisters in nutrient-rich conditions take up nutrients and grow slowly through a metabolism that is focused on ener-

gy production, although these cells could have utilized the available nutrient to adapt to the new conditions and ultimately grow faster. Still, their rudimentary metabolism accompanied by depleted metabolite pools (Figure 6) is sufficient to generate enough ATP to sustain non-growth associated maintenance costs (Figure 3D) and a high adenylate energy charge (Figure 3E). The proteome of *E.coli* persisters, which the starved cells try to, but do not, reach (Figure 4A) possibly due to lack of energy or carbon, does not show any signs of metabolic adaptation. Instead, the persister proteome is characterized by shift towards catabolism and stress response caused by the action of σ^S (Figure 5B). Likely due to the σ^S-shaped proteome and the sustained energy charge (Figure 3E), persisters in nutrient-rich conditions exhibit higher tolerance to certain antibiotics in comparison to starved cells (Figure 1B). On the basis of the generated data and the previous findings in the field, we developed a conceptual system-level model on the emergence of and sustenance in persistence.

According to this model, the state of persistence and the state of normal growth can be thought of as two attractors on a phenotypic landscape divided by a watershed (Figure 8). Moving on this landscape can on one hand be accomplished by changing the magnitude of metabolic fluxes, and on the other hand by altering the activity of growth-inhibiting mechanisms. Cells in metabolic homeostasis have high flux and low activity of growth-inhibiting mechanisms. Once the watershed is crossed, for instance through a

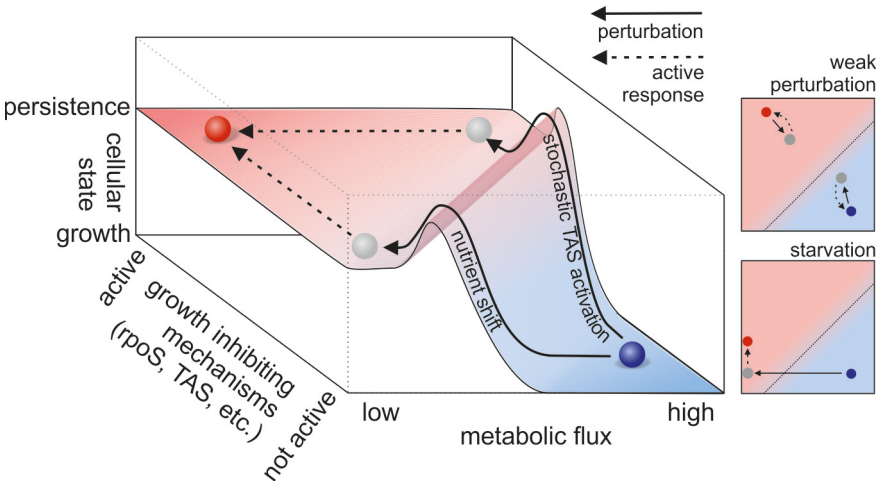

Figure 8: Schematic model: Persistence and growth are two attractor states on a phenotypic landscape with the dimensions 'metabolic flux' and 'activity of growth-inhibiting mechanisms'. The blue circle denotes the normal growth state, the red circle the persister state, the grey disk indicates the position of a cell directly after a perturbation. The magnitude of metabolic flux and the activity of growth-inhibiting mechanisms determine a cell's position on the landscape. If a cell is on the right side of the watershed (i.e. the hill / dotted line) it will move towards the attractor indicated by the blue disk and achieve normal growth in metabolic homeostasis. If a cell happens to be on the left side of the watershed, it will become a persister cell. Both states are achieved through active mechanisms (that eventually also require resources/ energy), as indicated by the finding that the persister state is not equal to the starved state. Various perturbations that were found to cause persistence (for instance, stochastic TAS induction, nutrient shift or diauxie) move the cell on the landscape in different directions, but all of them push it from the state of metabolic homeostasis beyond the watershed.

critically lowered metabolic flux (i.e. caused by a nutrient shift) or a critically increased activity of growth inhibiting mechanisms (i.e. through stochastic induction of TAS activity), cells will be attracted to the persister state. Achieving the ultimate persister state is an active process, which requires metabolic activity, active protein expression and thus presence of a carbon source. A perturbation that does not move the phenotypic state of the cell beyond the watershed will allow cells to restore metabolic homeostasis and continue to grow, not assuming the persister state.

Our model for persistence integrates the different (and at the first view contradicting) findings on persisters: while at the model's core is a flux-dependent feedback, there is a multitude of molecular mechanisms that can modulate the feedback. Because these two factors (metabolic flux and growth-inhibiting molecular mechanisms) can affect persister frequency, it is of crucial importance that they are both considered when investigating bacterial persistence. We envision that our developed model, which unifies the current and the newly obtained knowledge about persistence and creates a system-level view on persistence, will provide an important basis for future research towards understanding and eradicating persisters.

Accession codes

All mass spectrometry raw data files have been deposited to the ProteomeXchange Consortium (http://proteomecentral.proteomexchange.org) (identifier PXD001968).

Experimental procedures

Bacterial strains used in this study

Strain	**Source**
BW25113	Obtained from (Baba et al., 2006)
BW25113 Δrmf	Obtained from (Baba et al., 2006)
BW25113 ΔrelA	Obtained from (Baba et al., 2006)
BW25113 ΔrpoS	Obtained from (Baba et al., 2006)
BW25113 ΔrpoS + pNT3-rpoS	BW25113 ΔrpoS transformed with pNT3-rpoS plasmid from (Saka et al., 2005)
BW25113 + pBAD-LacY-EYFP	BW25113 transformed with pBAD-LacY-EYFP plasmid (gift from Jonas van der Berg)
MG1655	Obtained from (Maisonneuve et al., 2011)
MG1655 Δ10	Obtained from (Maisonneuve et al., 2011)
MG1655 Δ10ΔrpoS	MG1655 Δ10 with rpoS knock-out transduced with P1 phage from BW25113 ΔrpoS
MG1655 Δ10ΔrpoS + pNT3-dctA	MG1655 Δ10ΔrpoS transformed with pNTR-SD -dctA plasmid from (Saka et al., 2005)

Media and cultivation

Escherichia coli K12 strain BW25113 was used for the phenotypic characterization. Parts of the model validation were also done with the strain MG1655. All experiments were performed using M9 minimal medium, which was prepared as previously described (Kotte et al., 2014) or LB that was autoclaved and then fil-

tered through a 0.2 μm polyethersulfone (PES) filter. M9 medium was supplemented with a carbon source to a final concentration of 5 gL^{-1} glucose or 2 gL^{-1} fumarate, unless indicated otherwise. The carbon source stock solutions were made by dissolving the carbon source in demineralized water, adjusting the pH to 7 with NaOH or HCl, and filtering through a 0.2 μm PES filter. Cultivations were done in 50 mL of M9 medium in a 500 mL Erlenmeyer flask closed with a 38 mm silicone sponge closure (Bellco Glass) at 37 °C, 300 rpm, and 5 cm shaking diameter. On the following day, cells were diluted into a new culture prepared in the same way as the overnight culture, incubated and further diluted as needed in order to keep the cells in mid-exponential phase.

Flow cytometric analyses

Cell counts, fluorescence intensity and forward scatter values were determined with an Accuri C6 flow cytometer. Cells were diluted to an appropriate density with M9 medium without a carbon source directly prior to analysis. The flow cytometer was set to measure 20 μL volume, with the fluidics setting set to 'medium'. The SSC-H and FSC-H thresholds were set to 500 and 8000, respectively, in order to cut off most of the electronic noise. The Accuri CFlow Plus software was used for data analysis.

Antibiotic tolerance test

Cell were switched from M9 medium with glucose to M9 me-

dium with fumarate with (for time-course experiments with ampicillin) or without staining (for all other experiments), as described previously (Kotte et al., 2014). Staining was performed using the PKH-67 dye (Sigma-Aldrich). At various time points, antibiotics were added and the cells were incubated for 2 hours at 37 °C with shaking. Thereafter, 0.5 mL of the culture was transferred to 50 mL pre-warmed LB medium. Cells that resumed growth became bigger, and non-growing cells retained their size. The fraction of cells that do not resume growth was determined by observing cell size changes (with flow cytometry via forward scatter, a value which correlates with cell size) under the new conditions every 30 minutes from 0 to 4 hours after the transfer to LB medium. Then, fractions of non-recovering cells from the period between 2 and 3 hours were averaged for each replicate. A control experiment without antibiotics was performed, in order to measure the machine noise and the eventual fraction of non-recovering cells that died not due to antibiotic action, but due to the medium switch procedure. This level of non-recovering cells and noise was used to normalize the results.

Relative quantification of TAS transcripts abundance

To determine the relative amount of TAS transcripts, 0.9×10^9 cells growing on M9 medium supplemented with 5 gL^{-1} glucose, 1.6×10^9 cells switched to M9 medium without carbon source or supplemented with 2 gL^{-1} fumarate, and 0.9×10^9 cells growing on M9

medium supplemented with 5 gL^{-1} glucose that were treated in an identical way as during a nutrient switch were mixed in a 4:1 ratio with a 5% solution of phenol in ethanol (ice-cold) and incubated for 30 minutes on ice in order to stop RNA metabolism. Bacteria were then centrifuged (5', 8000g, 4°C), resuspended in the same volume of 1% solution of phenol in ethanol (ice-cold), centrifuged, (5', 8000g, 4°C), resuspended in the same volume of PBS (ice-cold) and centrifuged again (5', 8000g, 4°C). Pellets were then lysed with 150 µL of 1 mg mL-1 lysozyme solution in TE buffer (10 mM TRIS-HCl pH 8.0, 1 mM EDTA) for 5' at RT. Then, total RNA was extracted with 1 mL of Trizol (Invitrogen), followed by two extractions with 0.5 mL of chloroform. RNA was precipitated in 1 mL of 0.3 M sodium acetate 70% ethanol solution at -20°C for at least 16 h, pelleted by centrifugation (10', 12000g, 4°C) and washed twice with 1mL of 75% etOH. RNA was then dissolved in 20 µL of RNAse-free water, and treated with 3 U of DNAse I for 1 h at 37°C (Turbo DNA-free, Ambion/Applied Biosystems). After DNAse I inactivation, RNA integrity was assessed by agarose-TAE electrophoresis, and the yield and purity of the RNA determined by spectrophotometry (Nanodrop Instruments). Genomic DNA contamination of RNA samples was ruled out by performing a 30-cycle PCR reaction using gapA primer pair and 150 ng of RNA of each sample and verifying that no product was synthesized. For cDNA library construction, 1 µg of total RNA was reverse-transcribed with random hexamers using the High-capacity cDNA archive kit (Applied Biosystems) in a one-step run of 10

min at 25°C, 2 h at 37°C and 5 min at 85°C. For real-time quantitative PCR (qPCR) analysis, 2 ng of the cDNA library as template, 0.5 μM of each primer, and the Power Sybr Green PCR master mix (Applied Biosystems/Life Technologies) in a 10 μL final volume were used. qPCR reactions were performed in an ABI Prism 7300 instrument (Applied Biosystems) using the following program: 10 min at 95°C; 45 cycles of 15 sec at 95°C and 1 min at 60°C; dissociation curve of 15 sec at 95°C, 1 min at 60°C and a progressive temperature increase until 95°C. All qPCR runs included a non-template control, a mock cDNA library produced without reverse transcriptase, and a standard curve with different amounts cDNA. When feasible, primers were designed using Primer Express 3.0 (Applied Biosystems), and the quality of manually designed primers was examined with the same software. Primers are listed in Supplementary Table 7. For data analysis, the amplification efficiency in each qPCR assay was determined using a standard curve with 20, 4, 0.8, 0.16, 0.032, and 0 ng of cDNA run in parallel with the test samples. The baseline and threshold were set using the standard curve, and only cycle threshold (Ct) data from the samples lying within the linear range of the standard curve were considered. The Ct for every transcript in each sample corresponds to the mean value of the Cts obtained in three qPCR reactions run in parallel. Ct data from each sample was subtracted from the mean Ct value obtained from bacteria growing in M9 supplemented with glucose before the switch (ΔCt). These values were converted into relative fold-expression by raising

the amplification efficiency of each qPCR assay to the -ΔCt value. Expression data were further normalized to the mean relative expression value of 6 housekeeping genes (Supplementary Table 8).

$$r_{t_i} = \frac{S_{t_{i-1}} - S_{t_i}}{(t_{i-1} - t_i)\, X_{t_i}},$$

Relative expression was assessed in three independent biological replicates for each experimental condition.

Determination of fumarate uptake rate of persister cells.

To determine the fumarate uptake rate (FUR) of persister cells, exponentially growing *E. coli* cultures on M9 medium supplemented with glucose were harvested, centrifuged (10', 4000g, 4°C), washed twice with M9 medium containing no carbon source and re-suspended in M9 2g/L fumarate medium resulting in a cell concentration from 1 x 10^9 mL^{-1} to 5 x 10^9 mL^{-1}. The new cultures were incubated, and samples were taken over a period of 8 hours. Cell counts in the samples were determined by flow cytometry. For each sample, the medium was centrifuged (5', 4000g), filtered through a Spin-X centrifuge filter (Corning, 0.22 μm nylon membrane, 3s, 4000g), and stored at 4 °C. Fumarate concentration was determined by HPLC using a Hi-Plex H ion exchange column (MP: 0.005 M H_2SO_4, 0.6 mL/min, isocratic) and detection of UV absorbance at 210 nm. The fumarate concentration was then deter-

mined with a calibration curve prepared freshly for each experiment by dissolving appropriate amounts of sodium fumarate in M9 medium. The time-specific uptake rate was calculated as follows: where S is the fumarate concentration, t is the time elapsed from the beginning of the experiment, and X is the cell count. Then, a generalized additive model using univariate penalized cubic regression spline smooths with 8 knots was fitted to the data using R in order to estimate the mean and error values.

Determination of oxygen and carbon dioxide transfer rates of persister cells

E. coli cultures were prepared as for fumarate uptake rate determination. All experiments were performed in technical triplicates using the Respiration Activity Monitoring System (RAMOS) in special flasks filled with 26 mL of medium, shaken at 300 rpm. Cell counts and fumarate uptake rate were determined in parallel in a separate flask at an identical cell density. 10 minutes of rinsing time and 50 minutes of measurement time in the RAMOS device were used. Then, a generalized additive model was fit to the data using R in order to estimate the mean and error values as for fumarate uptake rate estimation.

Determination of fumarate uptake rate, and oxygen and carbon dioxide transfer rates in growing cells

To determine the fumarate uptake rate of cells exponentially growing on fumarate, a culture containing fumarate-adapted cells was diluted to a cell concentration that allowed for about 20 hours of growth before fumarate depletion. About 8 hours prior to fumarate depletion, samples were taken every 30 minutes. Cell counts in the cultures were determined by flow cytometry. Samples for determination of fumarate concentration were taken and analyzed with HPLC-UV as for persister cells. In parallel to the culture made for fumarate uptake rate determination, three cultures (technical triplicates) were made to measure oxygen and carbon dioxide transfer rates. All experiments were performed using the Respiration Activity Monitoring System (RAMOS) in special flasks filled with 26 mL of medium, shaken at 300 rpm. 10 minutes of rinsing time and 20 minutes of measurement time were used. All calculations were performed by the software package provided with the RAMOS system, which returned time-specific total carbon dioxide and total oxygen transfer values. The fumarate concentration-dependent fumarate uptake rate, fumarate concentration-dependent oxygen transfer rate, fumarate concentration-dependent carbon dioxide transfer rate, and fumarate-concentration dependent growth rate were determined by fitting the

cell counts and fumarate concentration measurements, as well as the cumulative oxygen transfer and carbon dioxide transfer values to a model describing exponential growth of cells with a fumarate concentration-dependent growth rate following Monod kinetics:

$$\frac{dX}{dt} = \mu X,$$

$$\frac{dS}{dt} = -\frac{1}{Y_{XS}}\mu X,$$

$$\frac{dO}{dt} = \frac{1}{Y_{OS}}\mu X,$$

$$\frac{dC}{dt} = \frac{1}{Y_{CS}}\mu X,$$

$$\mu = \frac{\mu_{max}\, S}{K_S + S},$$

where μ is the growth rate, S the fumarate concentration, X the cell count, O cumulative oxygen transfer, C cumulative CO_2 transfer, μ_{max} the maximum growth rate, K_s the Monod constant, Y_{XS} the cell count / fumarate yield, Y_{OS} cell count / oxygen yield and Y_{XS} the cell count / carbon dioxide yield. The fitting was performed in Matlab, using MCMC toolkit (Haario et al., 2006). The fumarate uptake rate, oxygen transfer rate and carbon dioxide transfer rate of growing cells were then determined with the estimated parameter values (± SD):

$\mu_{max} = 0.99 \pm 0.05$ [h^{-1}]

$K_S = 1.53 \pm 0.18$ [g L^{-1}]

$Y_{XS} = 0.90 \times 10^{12} \pm 0.15 \times 10^{12}$ [g^{-1}]

$Y_{OS} = 1.83 \times 10^{10} \pm 0.58 \times 10^{10}$ [mol^{-1}]

$Y_{CS} = 1.11 \times 10^{10} \pm 0.31$ [mol^{-1}]

and the following equations, for $2gL^{-1}$ fumarate concentration:

$$r_S(S) = \frac{1}{Y_{XS}} \frac{\mu_{max} S}{K_S + S}.$$

$$r_O(S) = \frac{1}{Y_{OS}} \frac{\mu_{max} S}{K_S + S}.$$

$$r_C(S) = \frac{1}{Y_{CS}} \frac{\mu_{max} S}{K_S + S}.$$

Cell volume determination

Cell volume was determined by microscopy imaging of live *E.coli* expressing a photo-switchable EYFP. LacY-EYFP fusion expression from pBAD-LacY-EYFP plasmid was induced in various ways, depending on the condition, in which cells were grown. In case of glucose-growing cells this was done with addition of 0.02% arabinose 12 hours prior to the measurements. This induction was enough to ensure high enough levels of LacY-EYFP expression in cells that were subsequently switched to medium with fumarate or medium without a carbon source, without further induction in the new conditions. In fumarate-growing cells, no induction was necessary and the leaky expression of protein was sufficient for imaging. Microscope imaging was performed as described before (Biteen et al., 2008). Localization of the LacY protein indicating the localization of cell membrane was digitized by manually selecting pixels on one side of longer cell axis, using ImageJ. The point coordinates

were then transformed in the XY coordinate system, so the longer cell axis laid on the X axis of the system. Simpson's rule was used to calculate individual cell volumes equal to the volume of a solid of revolution (i.e. a solid created by rotating the transformed points around the X axis).

ppGpp concentration determination

ppGpp was quantified as described before (Traxler et al., 2008), with slight modifications. Cultures were prepared as for fumarate uptake rate determination. At least $2\sigma 10^{10}$ cells (with the exact number determined with flow cytometry) were harvested by removing the culture medium through fast filtration (<60 s, 0.2 μm nylon membrane filter, Sigma) and placing the filter with cells immediately (<5s) into 3 mL of 1M formic acid pre-cooled to 0 °C. The filters containing *E. coli* cells were rinsed by pipetting the formic acid over the side of the filter containing the cells until all the cells were re-suspended, and cells were further incubated without the filter for 30-60 minutes in the formic acid at 0 °C. After that, the cell suspension was centrifuged (1 min, 21000 g, 4 °C) and the cell pellet was discarded. Water and formic acid were removed by freeze-drying overnight. The dried metabolites were then re-suspended in 0.13 mL of 0.1 M formic acid by vortexing and ultra-sonication, centrifuged (1 min, 21000 g, 4 °C), filtered through a Spin-X centrifuge filter (Corning, 0.22 μm nylon membrane, 3 s, 4000 g) and analyzed using a HPLC-UV method with absorbance measurement at 260 nm.

A PL-SAX anion exchange column (Agilent) was used at a column temperature of 60 °C. A 35 min linear gradient of two solvents was employed: 0': 100% A; 30': 0% A; 33': 0% A; 33': 100% A, where A: 0.01M K_2HPO_4, pH 2.6, B: 0.5M K_2HPO_4, pH 3.5. The flow rate was 1 mL/min. Peaks were quantified based on a ppGpp standard curve (Jena Biosciences) prepared in 0.1M formic acid and the intracellular concentrations were calculated considering the number of cells harvested and the determined cell volumes.

Metabolite concentration determination with LC-MS/MS

Cultures were prepared as for fumarate uptake rate determination. At least $2\sigma10^9$ cells (with the exact number determined with flow cytometry) were harvested by removing the medium through fast filtration (<60s, 0.2 μm nylon membrane filter, Sigma) and placing the filters with cells immediately (<5 s) into 3 mL of acetonitrile, methanol, water and formic acid (40:40:19.9:0.1 by volume) pre-cooled to -20 °C and with $U^{13}C$ internal standard (see below) spiked in. The filters containing *E. coli* cells were then incubated for 60-120 min in the mixture at -20 °C, and at the end of incubation time rinsed by pipetting the extraction mixture over the side of the filter containing cells, until all the cells were removed from the filter. The mixture was gathered and centrifuged (10', 21000g, 4°C). Organic solvents were removed from the supernatant in a vacuum concentrator (2h, RT) and the remaining water was removed by freeze-dry-

ing overnight. The samples were then resuspended in water by vortexing and ultra-sonication, and centrifuged (2', 21000g, 4°C) and analysed using a UHPLC-MS/MS method (injection volume of 10 µL). Quantification was done by relating the samples' $^{12}C/^{13}C$ peak area ratios to calibration curves constructed using pure ^{12}C standard in conjunction with the global $U^{13}C$ internal standard. The UHPLC-MS/MS system consisted of a Dionex Ultimate 3000 RS UHPLC (Dionex, Germering, Germany) with the sample compartment permanently cooled to 4°C, a Waters Acquity UPLC HSS T3 column with precolumn (dimensions: 150 mm×2.1 mm, particle size: 3 µM; Waters, Milford, MA, USA) was used at 50 °C column temperature. A linear binary UHPLC gradient was employed: 0': 100%A; 5': 100%A 10': 98%A; 11': 91%A; 16': 91%A; 18': 75%A, 22': 75%A; 22': 0%A; 26': 0%A; 26': 100%A; 30': 100%A, where Solvent A was composed of water:MeOH 95:5, 10 mM tributylamine (2.4 mL per L), 15 mM acetic acid (0.86 mL per L), 1 mM 3,5-Heptanedione (0.237 mL per L), and solvent B was isopropanol. The flow rate was 0.35 mL/min. Quantification was done via multiple reaction monitoring on a MDS Sciex API365 tandem mass spectrometer upgraded to EP10+ (Ionics, Bolton, Ontario, Canada) and equipped with a Turbo-Ionspray source (MDS Sciex, Nieuwerkerk aan den Ijssel, Netherlands). The source parameters were as following: NEB (nebulizing gas, N_2): 12 a.u., CUR (curtain gas, N_2): 12 a.u., CAD (collision-activated dissociation gas): 4 a.u., IS (ion spray voltage): -4500 V, TEM (temperature): 500 °C. If concentrations were measured in multiple campaigns, the

data was analyzed with a mixed effects model using the campaign as a nuisance variable. Otherwise, mean and standard error were calculated normally. The ^{13}C internal standard was prepared by growing *Saccharomyces cerevisiae* on ^{13}C uniformly-labelled glucose (Cambridge Isotope Labs) as a sole carbon source followed by quenching and metabolite extraction as described before (Siegel et al., 2014).

Absolute protein quantification

$1.5x10^9$ growing, persister or starved cells were centrifuged (1', 16000 g, 4 °C), washed twice with ice-cold PBS, and the cell pellet was frozen in liquid nitrogen. Cell pellets were lysed in 50 μl lysis buffer (2% sodiumdoxycholate, 0.1M ammoniumbicarbonate) and disrupted by two cycles of sonication for 20 seconds (Hielscher Ultrasonicator). Protein concentration was determined by BCA assay (Thermo Fisher Scientific) using a small sample aliquot. Proteins were reduced with 5 mM TCEP for 15 min at 95°C, alkylated with 10 mM iodoacetamide for 30 min in the dark at room temperature and quenched with 12.5 mM N-acetyl-cysteine. Samples were diluted with 0.1M ammoniumbicarbonate solution to a final concentration of 1% sodiumdoxycholate before digestion with trypsin (Promega) at 37 °C overnight (protein to trypsin ratio: 50:1). After digestion, the samples were supplemented with TFA to a final concentration of 0.5% and HCl to a final concentration of 50 mM. Precipitated sodiumdoxycholate was removed by centrifugation (15 minutes at

4°C at 14,000 rpm). Then, peptides were desalted on C18 reversed phase spin columns according to the manufacturer's instructions (Macrospin, Harvard Apparatus), dried under vacuum and stored at -80°C until further processing.

1 µg of peptides of each sample were subjected to LC–MS analysis using a dual pressure LTQ-Orbitrap Velos mass spectrometer connected to an electrospray ion source (both Thermo Fisher Scientific) as described recently (Glatter et al., 2012) with a few modifications. In brief, peptide separation was carried out using an EASY nLC-1000 system (Thermo Fisher Scientific) equipped with a RP-HPLC column (75 µm × 45 cm) packed in-house with C18 resin (ReproSil-Pur C18–AQ, 1.9 µm resin; Dr. Maisch GmbH, Ammerbuch-Entringen, Germany) using a linear gradient from 95% solvent A (0.15% formic acid, 2% acetonitrile) and 5% solvent B (98% acetonitrile, 0.15% formic acid) to 28% solvent B over 90 min at a flow rate of 0.2 µl/min. The data acquisition mode was set to obtain one high resolution MS scan in the FT part of the mass spectrometer at a resolution of 120,000 full width at half-maximum (at m/z 400) followed by MS/MS scans in the linear ion trap of the 20 most intense ions. The charged state screening modus was enabled to exclude unassigned and singly charged ions and the dynamic exclusion duration was set to 20s. The ion accumulation time was set to 300 ms (MS) and 50 ms (MS/MS).

For label-free quantification, the generated raw files were imported into the Progenesis LC-MS software (Nonlinear Dynam-

ics, Version 4.0) and analyzed using the default parameter settings. MS/MS-data were exported directly from Progenesis LC-MS in mgf format and searched against a decoy database of the forward and reverse sequences of the predicted proteome from *E. coli* (Uniprot, download date: 15/6/2012, total of 10,388 entries) using MASCOT. The search criteria were set as following: full tryptic specificity was required (cleavage after lysine or arginine residues); 3 missed cleavages were allowed; carbamidomethylation (C) was set as fixed modification; oxidation (M) as variable modification. The mass tolerance was set to 10 ppm for precursor ions and 0.6 Da for fragment ions. Results from the database search were imported into Progenesis and the protein false discovery rate (FDR) was set to 1% using the number of reverse hits in the dataset. The final protein lists containing the summed peak areas of all identified peptides for each protein, respectively, were exported from Progenesis LC-MS and further statically analyzed using an in-house developed R script (SafeQuant) (Glatter et al., 2012).

Principal component analysis and GOterm enrichment analysis

First, we applied 2-dimensional principal component analysis (without scaling) using the FactoMineR package for R to datasets describing relative fold-difference in protein concentrations between all the analysed conditions (14 conditions or 3 conditions at the same time). PCA analysis assigned two coordinates (one for

each dimension) based on correlation coefficients calculated between each and every of the analyzed proteomes. These coordinates placed each of the analyzed proteomes in a 2-dimensional space. Proteomes not generated in this study were then projected on the 2-dimensional PCA space. This PCA space was generated based on the proteomes measured in this study but only using a subset of proteins that measured both in this and the external study. Furthermore, for each protein and each of the 2 new PCA dimensions a correlation coefficient was calculated between: (1) a numerical vector containing the particular protein concentration fold-change values between each of the analyzed proteomes and (2) a numerical vector containing the coordinate along the particular PCA dimension of each of the analyzed proteomes. These correlation coefficients indicate if an increase or decrease in each protein concentration correlates with the position of the proteome along the dimensions of the PCA space. Along each correlation coefficient, a p-value indicating whether this correlation coefficient is significantly different from 0 was calculated. Then, we created (for each of the two PCA dimensions) two lists containing the protein names and p-values of their positive or negative correlation coefficients, thus enabling us to distinguish to which direction of the PCA dimension they contribute (the negatively correlated proteins contribute in an opposite direction than the positively correlated proteins). Then, these lists were supplemented with protein names that do not contribute to the particular direction of the PCA dimension (i.e. a list with proteins

positively correlated with dimension 1 was supplemented with a list of proteins negatively correlated with dimension 1), with p-value of these added proteins set to 1. This supplementation was done in order to include all the measured proteins in GOterm enrichment analysis described below.

GOterm enrichment analysis was performed using the TopGO package for R. GOterm-gene annotations were downloaded from Bioconductor (the org.Eck12.eg.db database). A protein was selected as significant if the p-value of its correlation coefficient (see above) was lower than 0.1. Then, GOterms were assigned using the elim algorithm, which walks through GOterm hierarchy from the highest to the lowest level of detail, eliminating broad GOterms given that more detailed, child GOterms were selected. For every GOterm, we determined significance of its enrichment using the GOtTest function (which considered the number of significant proteins including their p-values), and thereby we created a ranked list of the enriched GOterms.

Enrichment analyses of sigma factor, transcription factor and sRNA activity

Activity of sigma factors, transcription factors and sRNA was determined as previously described with small adaptations (Zampar et al., 2013). Specifically, the subsets of regulated proteins were selected by clustering performed with STEM software (version

1.3.8) (Ernst and Bar-Joseph, 2006), which first generated a set of random model expression profiles (representing protein concentration change over time). Then, protein expression profiles were assigned to the random model expression profiles based on their correlation to these profiles. Random model expression profiles with statistically significant number of protein profiles assigned to them were then clustered depending on how well they correlated with each other. This resulted in lists of proteins that changed their concentrations significantly during the time course, clustered along similar expression profiles. The settings used for analysis can be found in **Supplementary Table** 9. For enrichment analysis of sigma factor activity, we used sigma factor-gene associations, transcription factor-gene associations or sRNA-gene associations from the RegulonDB database which were supported by experimental evidence. For each tested factor *j*, a p-value based on a hyper-geometric mean was calculated:

$$p_j = 1 - \sum_{i=0}^{k_j-1} \frac{\binom{M_j}{i}\binom{N-M_j}{n-i}}{\binom{N}{n}},$$

where N is the total number of proteins, n - number of proteins in the investigated subset, M_j - number of proteins associated with sigma factor *j* in the complete protein list, k_j – number of proteins associated with sigma factor *j* in the investigated subset. The p-value, after False Discovery Rate adjustment, is equal to the probability that the observed protein expression change occurred by chance and not because of a real regulatory effect of the investigated sigma factor.

Determination of fraction of persisters and growing cells

Cell were switched from M9 medium with glucose to M9 medium with fumarate as described previously, with staining (Kotte et al., 2014). Staining was performed using the PKH-67 dye (Sigma-Aldrich). Multiple cell count and fluorescence intensity measurements were taken during the culturing period. The fraction of growing and non-growing cells after the shift was determined by fitting a model of two Gaussian distributions and of exponential growth to the measured fluorescence intensity, as described before (Kotte et al., 2014).

Estimation of maximum ATP production rate with flux balance analysis

A stoichiometric genome-scale metabolic network model of *E.coli* metabolism (Reed et al., 2003) was constrained with the measured extracellular rates (carbon uptake, gas exchange and biomass production) within their 99.5% confidence intervals. The units of measured rates were converted from [fmol $cell^{-1}$ h^{-1}] to [mmol gDW^{-1} h^{-1}] using the measured cell volumes and assuming that 0.74 of cell mass is water (Ishkawa et al., 1995) and that the average cell density is 1.105 kg L^{-1}. The model was solved using GAMS with maximization of ATP hydrolysis rate as the objective.

Acknowledgments

We thank E. Wit and B. Niebel for help with statistical analysis; A. van Dam and H. Permentier for help with metabolite quantification; A. Robinson for help with microscopy; K. Gerdes, E. Maisonneuve, M. Askvad Sørensen, A. Papagiannakis, K.E.S. Leupold, T. Kimkes for discussions and critically reviewing an earlier version of the manuscript, and H. Schramke for discussions and critically reviewing this manuscript. We also thank members of the MSB group for support. The work was funded with NWO-Vidi grant to MH.

Reference List

Amato, S.M., and Brynildsen, M.P. (2015). Persister Heterogeneity Arising from a Single Metabolic Stress. Current Biology *25,* 2090-2098.

Amato, S.M., and Brynildsen, M.P. (2014). Nutrient Transitions Are a Source of Persisters in Escherichia coli Biofilms. Plos One *9,* e93110.

Amato, S.M., Fazen, C.H., Henry, T.C., Mok, W.W.K., Orman, M.A., Sandvik, E.L., Volzing, K.G., and Brynildsen, M.P. (2014). The role of metabolism in bacterial persistence. Front. Microbiol. *5,* 70.

Amato, S.M., Orman, M.A., and Brynildsen, M.P. (2013). Metabolic Control of Persister Formation in Escherichia coli. Mol. Cell *50,* 475-487.

Appelberg, R. (2006). Macrophage nutriprive antimicrobial mechanisms. J. Leukoc. Biol. *79,* 1117-1128.

Baba, T., Ara, T., Hasegawa, M., Takai, Y., Okumura, Y., Baba, M., Datsenko, K.A., Tomita, M., Wanner, B.L., and Mori, H. (2006). Construction of Escherichia coli K-12 in-frame, single-gene knockout mutants: the Keio collection. Molecular Systems Biology *2,* 2006.0008.

Balaban, N.Q., Gerdes, K., Lewis, K., and McKinney, J.D. (2013). A problem of persistence: still more questions than answers? Nature Reviews Microbiology *11,* 587-591.

Berthoumieux, S., de Jong, H., Baptist, G., Pinel, C., Ranquet, C., Ropers, D., and Geiselmann, J. (2013). Shared control of gene expression in bacteria by transcription factors and global physiology of the cell. Molecular Systems Biology *9: 634*

Biteen, J.S., Thompson, M.A., Tselentis, N.K., Bowman, G.R., Shapiro, L., and Moerner, W.E. (2008). Super-resolution imaging in live Caulobacter crescentus cells using photoswitchable EYFP. Nat. Methods *5,* 947-949.

Cam, K., Rome, G., Krisch, H.M., and Bouche, J.P. (1996). RNase E processing of essential cell division genes mRNA in Escherichia coli. Nucleic Acids Res. *24,* 3065-3070.

Chapman, A.G., Fall, L., and Atkinson, D.E. (1971). Adenylate Energy Charge in Escherichia-Coli during Growth and Starvation. J. Bacteriol. *108,* 1072-1086.

Cheng, Z.F., and Deutscher, M.P. (2005). An important role for RNase R in mRNA decay. Mol. Cell *17,* 313-318.

Cheng, Z.F., and Deutscher, M.P. (2002). Purification and characterization of the Escherichia coli exoribonuclease RNase R - Comparison with RNase II. J. Biol. Chem. *277,* 21624-21629.

Cho, J., Rogers, J., Kearns, M., Leslie, M., Hartson, S.D., and Wilson, K.S. (2015). Escherichia coli persister cells suppress translation by selectively disassembling and degrading their ribosomes. Mol. Microbiol. *95,* 352-364.

Cohen, N., Lobritz, M., and Collins, J. (2013). Microbial Persistence and the Road to Drug Resistance. Cell Host & Microbe *13,* 632-642.

Dawson, C.C., Intapa, C., and Jabra-Rizk, M.A. (2011). "Persisters": Survival at the Cellular Level. PLoS Pathog. *7,* e1002121.

Ernst, J., and Bar-Joseph, Z. (2006). STEM: a tool for the analysis of short time series gene expression data. BMC Bioinformatics *7,* 191.

Fauvart, M., De Grootet, V.N., and Michiels, J. (2011). Role of persister cells in chronic infections: clinical relevance and perspectives on anti-persister therapies. J. Med. Microbiol. *60,* 699-709.

Feng, J., Kessler, D.A., Ben-Jacob, E., and Levine, H. (2014). Growth feedback as a basis for persister bistability. Proc. Natl. Acad. Sci. U. S. A. *111,* 544-549.

Friedman, D.I. (1988). Integration Host Factor - a Protein for all Reasons. Cell *55,* 545-554.

Fung, D.K.C., Chan, E.W.C., Chin, M.L., and Chan, R.C.Y. (2010). Delineation of a Bacterial Starvation Stress Response Network Which Can Mediate Antibiotic Tolerance Development. Antimicrob. Agents Chemother. *54,* 1082-1093.

Gentry, D.R., Hernandez, V.J., Nguyen, L.H., Jensen, D.B., and Cashel, M. (1993). Synthesis of the Stationary-Phase Sigma-Factor Sigma(s) is Positively Regulated by Ppgpp. J. Bacteriol. *175,* 7982-7989.

Glatter, T., Ludwig, C., Ahrne, E., Aebersold, R., Heck, A.J.R., and Schmidt, A. (2012). Large-Scale Quantitative Assessment of Different In-Solution Protein Digestion Protocols Reveals Superior Cleavage Efficiency of Tandem Lys-C/Trypsin Proteolysis over Trypsin Digestion. J. Proteome Res. *11,* 5145-5156.

Grant, S.S., and Hung, D.T. (2013). Persistent bacterial infections, antibiotic tolerance, and the oxidative stress response. Virulence *4,* 273-283.

Guarner, F., and Malagelada, J. (2003). Gut flora in health and disease. The Lancet *361,* 512-519.

Haario, H., Laine, M., Mira, A., and Saksman, E. (2006). DRAM: Efficient adaptive MCMC. Statistics and Computing *16,* 339-354.

Hardiman, T., Lemuth, K., Keller, M.A., Reuss, M., and Siemann-Herzberg, M. (2007). Topology of the global regulatory network of carbon limitation in Escherichia coli. J. Biotechnol. *132,* 359-374.

Haseltine, W., and Block, R. (1973). Synthesis of Guanosine Tetraphosphate and Pentaphosphate Requires Presence of a Codon-Specific, Uncharged Transfer Ribonucleic-Acid in Acceptor Site of Ribosomes - (Stringent Control Ppgpp (Msi) and Pppgpp (Msii) Protein Synthesis Escherichia-Coli). Proc. Natl. Acad. Sci. U. S. A. *70,* 1564-1568.

Ishkawa, H., Shimoda, M., Shiratsuchi, H., and Osajima, Y. (1995). Sterilization of microorganisms by the supercritical carbon dioxide micro-bubble method. Bioscience Biotechnology and Biochemistry *59,* 1949-1950.

Kaguni, J.M., Bertsch, L.L., Bramhill, D., Flynn, J.E., Fuller, R.S., Funnell, B., Maki, S., Ogawa, T., Ogawa, K., and van der Ende, A. (1985). Initiation of replication of the Escherichia coli chromosomal origin reconstituted with purified enzymes. Basic Life Sci. *30,* 141-150.

Kaplan, R., and Apirion, D. (1974). Involvement of Ribonuclease-I, Ribonuclease-Ii, and Polynucleotide Phosphorylase in Degradation of Stable Ribonucleic-Acid during Carbon Starvation in Escherichia-Coli. J. Biol. Chem. *249,* 149-151.

Keren, I., Shah, D., Spoering, A., Kaldalu, N., and Lewis, K. (2004). Specialized persister cells and the mechanism of multidrug tolerance in Escherichia coli. J. Bacteriol. *186,* 8172-8180.

Kiviet, D.J., Nghe, P., Walker, N., Boulineau, S., Sunderlikova, V., and Tans, S.J. (2014). Stochasticity of metabolism and growth at the single-cell level. Nature *514,* 376-379.

Klumpp, S., Zhang, Z., and Hwa, T. (2009). Growth Rate-Dependent Global Effects on Gene Expression in Bacteria. Cell *139,* 1366-1375.

Kochanowski, K., Volkmer, B., Gerosa, L., van Rijsewijk, B.R.H., Schmidt, A., and Heinemann, M. (2013). Functioning of a metabolic flux sensor in Escherichia coli. Proc. Natl. Acad. Sci. U. S. A. *110,* 1130-1135.

Korch, S.B., and Hill, T.M. (2006). Ectopic overexpression of wild-type and mutant hipA genes in Escherichia coli: Effects on macromolecular synthesis and persister formation. J. Bacteriol. *188,* 3826-3836.

Kotte, O., Volkmer, B., Radzikowski, J.L., and Heinemann, M. (2014). Phenotypic bistability in Escherichia coli's central carbon metabolism. Molecular Systems Biology *10,* 736.

Lewis, K., Naroditskaya, V., Ferrante, A., and Fokina, I. (1994). Bacterial-Resistance to Uncouplers. J. Bioenerg. Biomembr. *26,* 639-646.

Lewis, K. (2010). Persister Cells. Annu. Rev. Microbiol. *64,* 357-372.

Maisonneuve, E., Castro-Camargo, M., and Gerdes, K. (2013). (p)ppGpp Controls Bacterial Persistence by Stochastic Induction of Toxin-Antitoxin Activity. Cell *154,* 1140-1150.

Maisonneuve, E., Shakespeare, L.J., Jorgensen, M.G., and Gerdes, K. (2011). Bacterial persistence by RNA endonucleases. Proc. Natl. Acad. Sci. U. S. A. *108*, 13206–13211

Montero, M., Rahimpour, M., Viale, A.M., Almagro, G., Eydallin, G., Sevilla, A., Canovas, M., Bernal, C., Belen Lozano, A., Jose Munoz, F. *et al.* (2014). Systematic Production of Inactivating and Non-Inactivating Suppressor Mutations at the relA Locus That Compensate the Detrimental Effects of Complete spoT Loss and Affect Glycogen Content in Escherichia coli. Plos One *9,* e106938.

Nguyen, D., Joshi-Datar, A., Lepine, F., Bauerle, E., Olakanmi, O., Beer, K., McKay, G., Siehnel, R., Schafhauser, J., Wang, Y., Britigan, B.E., and Singh, P.K. (2011). Active Starvation Responses Mediate Antibiotic Tolerance in Biofilms and Nutrient-Limited Bacteria. Science *334,* 982-986.

Nusslein-Crystalla, V., Niedenhof, I., and Rein, R. (1982). Dnac-Dependent Reconstitution of Replication Forks in Escherichia-Coli Lysates. J. Bacteriol. *150,* 286-292.

Orth, J.D., Conrad, T.M., Na, J., Lerman, J.A., Nam, H., Feist, A.M., and Palsson, B.O. (2011). A comprehensive genome-scale reconstruction of Escherichia coli metabolism-2011. Molecular Systems Biology *7,* 535.

Radzikowski, J.L., Vedelaar, S., Siegel, D., Ortega, ÁD., Schmidt, A., and Heinemann, M. (2016). Bacterial persistence is an active σ^S stress response to metabolic flux limitation. Mol Syst Biol *12,* 882

Reed, J.L., Vo, T.D., Schilling, C.H., and Palsson, B.O. (2003). An expanded genome-scale model of Escherichia coli K-12 (iJR904 GSM/GPR). Genome Biol. *4,* R54.

Rohmer, L., Hocquet, D., and Miller, S.I. (2011). Are pathogenic bacteria just looking for food? Metabolism and microbial pathogenesis. Trends Microbiol. *19,* 341-348.

Saka, K., Tadenuma, M., Nakade, S., Tanaka, N., Sugawara, H., Nishikawa, K., Ichiyoshi, N., Kitagawa, M., Mori, H., Ogasawara, N., and Nishimura, A. (2005). A complete set of Escherichia coli open reading frames in mobile plasmids facilitating genetic studies. Dna Research *12,* 63-68.

Salgado, H., Peralta-Gil, M., Gama-Castro, S., Santos-Zavaleta, A., Muniz-Rascado, L., Garcia-Sotelo, J.S., Weiss, V., Solano-Lira, H., Martinez-Flores, I., Medina-Rivera, A., *et al.* (2013). RegulonDB v8.0: omics data sets, evolutionary conservation, regulatory phrases, cross-validated gold standards and more. Nucleic Acids Res. *41,* D203-D213.

Schmidt, A., Kochanowski, K., Vedelaar, S., Ahrne, E., Volkmer, B., Callipo, L., Knoops, K., Bauer, M., Aebersold, R., and Heinemann, M. (2016). The quantitative and condition-dependent Escherichia coli proteome. Nat. Biotechnol. *34,* 104-110.

Shah, D., Zhang, Z., Khodursky, A., Kaldalu, N., Kurg, K., and Lewis, K. (2006). Persisters: a distinct physiological state of E-coli. Bmc Microbiology *6,* 53.

Shimizu, K. (2013). Regulation Systems of Bacteria such as Escherichia coli in Response to Nutrient Limitation and Environmental Stresses. Metabolites *4,* 1-35.

Siegel, D., Meinema, A.C., Permentier, H., Hopfgartner, G., and Bischoff, R. (2014). Integrated Quantification and Identification of Aldehydes and Ketones in Biological Samples. Anal. Chem. *86,* 5089-5100.

Tashiro, Y., Kawata, K., Taniuchi, A., Kakinuma, K., May, T., and Okabe, S. (2012). RelE-Mediated Dormancy Is Enhanced at High Cell Density in Escherichia coli. J. Bacteriol. *194*, 1169–1176

Traxler, M.F., Summers, S.M., Nguyen, H., Zacharia, V.M., Hightower, G.A., Smith, J.T., and Conway, T. (2008). The global, ppGpp-mediated stringent response to amino acid starvation in Escherichia coli. Mol. Microbiol. *68,* 1128-1148.

Xiao, H., Kalman, M., Ikehara, K., Zemel, S., Glaser, G., and Cashel, M. (1991). Residual Guanosine 3',5'-Bispyrophosphate Synthetic Activity of Rela Null Mutants can be Eliminated by Spot Null Mutations. J. Biol. Chem. *266,* 5980-5990.

Zampar, G.G., Kuemmel, A., Ewald, J., Jol, S., Niebel, B., Picotti, P., Aebersold, R., Sauer, U., Zamboni, N., and Heinemann, M. (2013). Temporal system-level organization of the switch from glycolytic to gluconeogenic operation in yeast. Molecular Systems Biology *9,* 651.

Supplementary Figures

Supplementary Figure 1 – Estimation of the effect of the small fraction of growing cells after a nutrient switch on the determined persister phenotype.

(A) Cell count measurements at multiple time points after the switch from glucose to 2 g L^{-1} fumarate, from 9 independent experiments. In these experiments, cells were stained with a fluorescent dye as described before (Kotte et al., 2014). Non-/slow-growing cells retain fluorescence, while it is halved in growing cells with each division, resulting in a bimodal distribution of fluorescence intensities in a population. The violet lines represent model fits characterizing the number of growing cells as performed before (Kotte et al., 2014). Specifically, the model fits a bi-Gaussian distribution to the dynamic fluorescence and the cell count data, and estimates the sizes of the sub-populations. Open circles – initial cell density, red circles – total cell count, violet line – growing cell fit (solid) or extrapolation of the fit (dashed). The grey bar represents 1% of the initial cell density. The intersects of the grey bar and the extrapolated growing cell fits show that the growing population reached 1% of the initial cell density approximately 10 to 15 hours after the switch. The estimated fraction of growing cells in the total measured population, in combination with the phenotype measurements of mixed population and the measurements of the phenotype of cells growing normally on fumarate were used to estimate the effect of the growing cells present in the population (cf. Supplementary Text S1). Panels (B-D) show a comparison of the mixed population measurements (grey bars) and the de-convoluted worst-case scenario (yellow bars) of (B) the growth rates, (C) the physiological rates, and (D) the metabolite concentrations. Error bars indicate 95% confidence intervals of the mean. Data from replicate experiments.

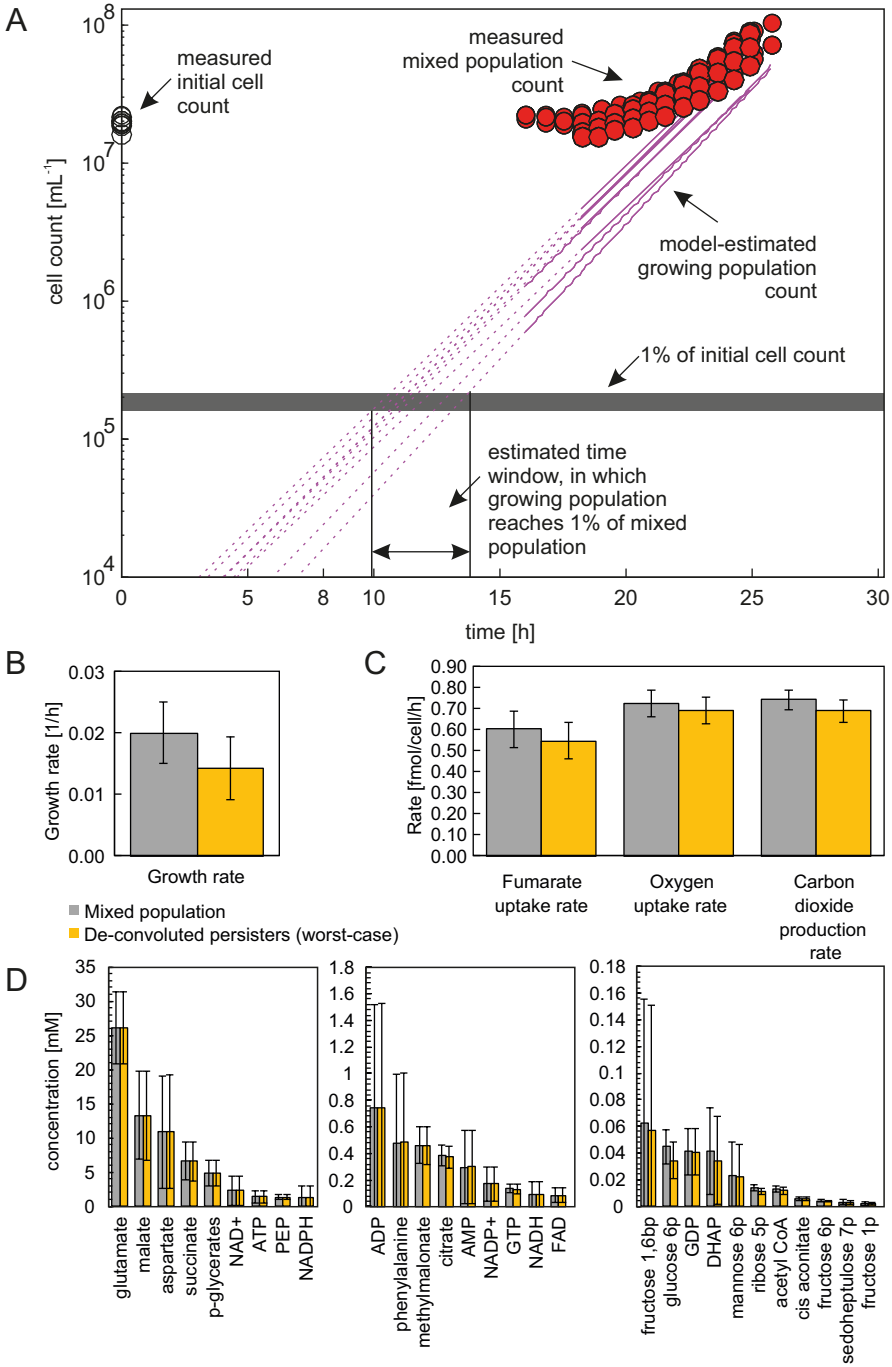
A
measured initial cell count
measured mixed population count
model-estimated growing population count
1% of initial cell count
estimated time window, in which growing population reaches 1% of mixed population
cell count [mL-1]
time [h]
B
Growth rate [1/h]
Growth rate
C
Rate [fmol/cell/h]
Fumarate uptake rate
Oxygen uptake rate
Carbon dioxide production rate
Mixed population
De-convoluted persisters (worst-case)
D
concentration [mM]
glutamate
malate
aspartate
succinate
p-glycerates
NAD+
ATP
PEP
NADPH
ADP
phenylalanine
methylmalonate
citrate
AMP
NADP+
GTP
NADH
FAD
fructose 1,6bp
glucose 6p
GDP
DHAP
mannose 6p
ribose 5p
acetyl CoA
cis aconitate
fructose 6p
sedoheptulose 7p
fructose 1p

Supplementary Figure 2 - Heat map of expression levels of proteins involved in E. coli central metabolic pathways.

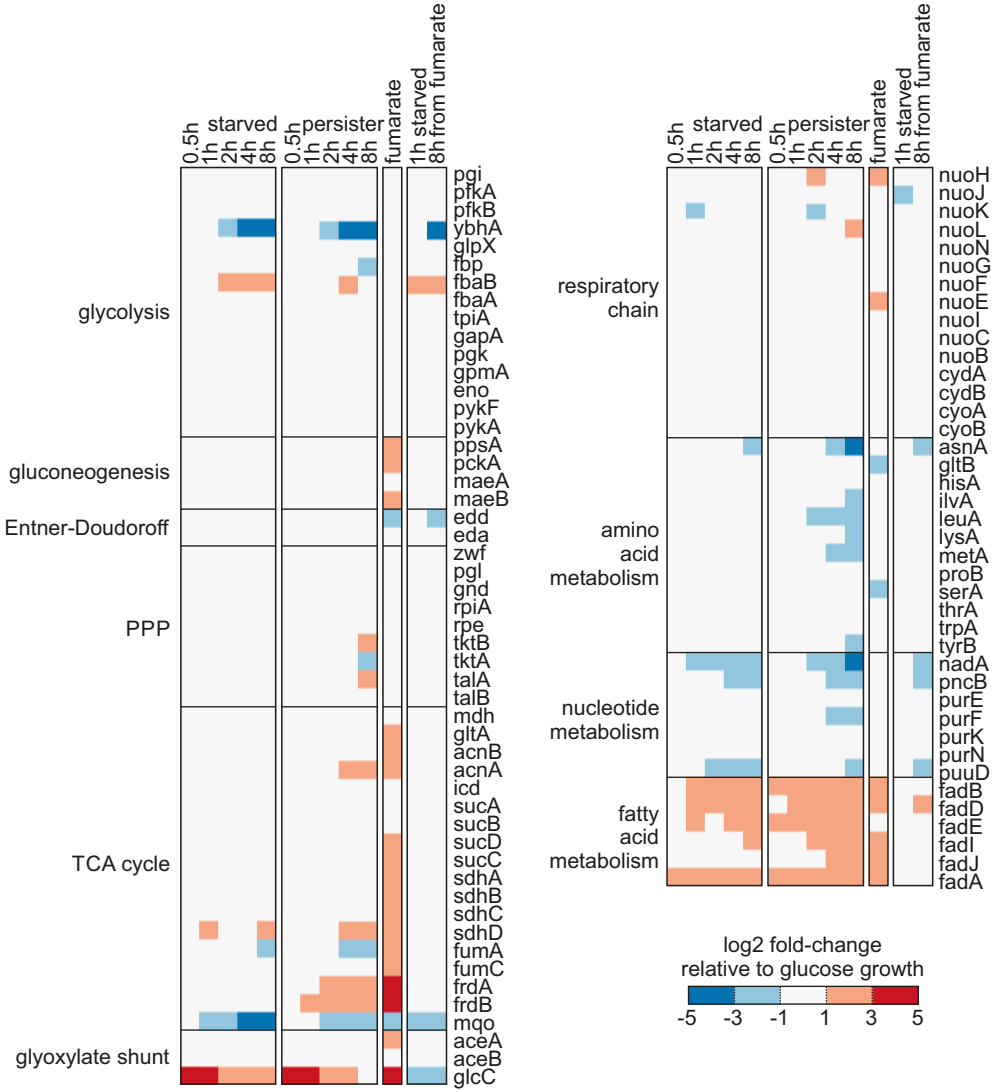

The data show log2-fold change of protein levels (relative to cells growing on glucose) in starved cells, persister cells, cells growing on fumarate and log2-fold change (relative to cells growing on fumarate) in cells starved from fumarate (in relation to fumarate). Gene lists for pathways were generated based on data from EcoCyc (Keseler et al., 2013). All genes with protein expression data available shown. White color indicates less than 2-fold change (i.e. log2-fold change between -1 and 1) in expression.

Supplementary Tables

Supplementary Table 1 – *E. coli* cell size on glucose, fumarate, as well as during entry into persistence and entry into starvation

condition [cell number]	mean volume [fL]	sd	mean width [um]	sd	mean length [um]	sd
fumarate [n=116]	1.11	0.58	0.89	0.18	2.45	0.55
glucose [n=104]	2.15	0.84	1.15	0.18	2.87	0.56
persister 0.5h [n=143]	0.89	0.34	0.88	0.12	2.11	0.55
persister 1h [n=154]	0.73	0.34	0.83	0.14	1.91	0.41
persister 2h [n=158]	0.55	0.26	0.76	0.14	1.72	0.40
persister 4h [n=183]	0.60	0.25	0.81	0.12	1.70	0.39
persister 8h [n=171]	0.61	0.26	0.81	0.13	1.73	0.44
starved 0.5h [n=138]	1.00	0.43	0.94	0.17	2.09	0.52
starved 1h [n=176]	0.71	0.45	0.85	0.17	1.73	0.51
starved 2h [n=155]	0.63	0.33	0.78	0.13	1.88	0.49
starved 4h [n=124]	0.75	0.39	0.86	0.16	1.80	0.45
starved 8h [n=172]	0.92	0.40	0.95	0.15	1.95	0.41

Cell volumes, widths and lengths in different conditions and time points measured with super-resolution microscopy. Number of analyzed cells (n) is indicated for each condition. The volumes were used for the determination of the intracellular metabolite concentrations.

Supplementary Table 2 – Physiological parameters of cells growing exponentially on fumarate, and in cells 8 hours after entry into persistence or starvation

	Cells growing on fumarate (2 g L^{-1})	**Persister cells**	**Starved cells**
Growth rate [h^{-1}]	0.56 ± 0.08	0.02 ± 0.005	-0.005 ± 0.005
Fumarate uptake rate [fmol $cell^{-1}$ h^{-1}]	5.47 ± 1.28	0.60 ± 0.08	N/A
Oxygen uptake rate [fmol $cell^{-1}$ h^{-1}]	3.07 ± 1.19	0.72 ± 0.05	N/A
Carbon dioxide production rate [fmol $cell^{-1}$ h^{-1}]	5.08 ± 1.77	0.74 ± 0.06	N/A

Physiological parameters of cells growing on 2 g L^{-1} fumarate, persister cells in fumarate medium 8 hours after the nutrient shift, and starved cells. Mean values and 95% confidence intervals of the mean shown.

Supplementary Table 3 – Metabolite concentrations during growth on glucose, fumarate, entry into persistence and starvation

condition	time [h]	compound	concentration [mM]	SEM [mM]	campaigns	biological replicates
fumarate	Ss	acetyl CoA	0.1177	0.0513	3	36
glucose	Ss	acetyl CoA	0.1514	0.0585	3	36
persister	0.5	acetyl CoA	0.0096	0.0016	4	24
persister	1	acetyl CoA	0.0078	0.0023	4	24
persister	2	acetyl CoA	0.0077	0.0020	4	24
persister	4	acetyl CoA	0.0116	0.0029	4	24
persister	8	acetyl CoA	0.0127	0.0012	4	24
starved	0.5	acetyl CoA	0.0176	0.0034	3	18
starved	1	acetyl CoA	0.0092	0.0019	3	18
starved	2	acetyl CoA	0.0047	0.0013	3	18
starved	4	acetyl CoA	0.0032	0.0014	3	18
starved	8	acetyl CoA	0.0035	0.0016	3	18
fumarate	Ss	ADP	0.5500	0.0161	2	24
glucose	Ss	ADP	0.3208	0.0791	2	24
persister	0.5	ADP	1.2352	0.2334	2	12
persister	1	ADP	1.5840	0.2852	2	12
persister	2	ADP	1.6277	0.2542	2	12
persister	4	ADP	1.1010	0.2134	2	12
persister	8	ADP	0.7451	0.3949	2	12
starved	0.5	ADP	1.5108	0.2418	2	12
starved	1	ADP	1.8463	0.1539	2	12
starved	2	ADP	1.9308	0.2741	2	12
starved	4	ADP	1.0505	0.0929	2	12
starved	8	ADP	0.5747	0.0716	2	12
fumarate	Ss	AMP	0.1043	0.0144	2	24
glucose	Ss	AMP	0.0575	0.0018	2	24
persister	0.5	AMP	0.3637	0.0261	2	12
persister	1	AMP	0.4711	0.0146	2	12
persister	2	AMP	0.5445	0.0680	2	12
persister	4	AMP	0.4443	0.0869	2	12
persister	8	AMP	0.2971	0.1389	2	12
starved	0.5	AMP	0.6418	0.0614	2	12
starved	1	AMP	1.1616	0.0775	2	12
starved	2	AMP	1.5936	0.2074	2	12
starved	4	AMP	1.8609	0.2381	2	12
starved	8	AMP	1.8475	0.3846	2	12
fumarate	ss	aspartate	2.4761	0.3916	3	36
glucose	ss	aspartate	0.7487	0.0697	3	36
persister	0.5	aspartate	9.7999	1.2402	4	24
persister	1	aspartate	15.2974	3.1304	4	24
persister	2	aspartate	22.6584	3.8710	4	24
persister	4	aspartate	20.0508	5.3433	4	24
persister	8	aspartate	10.8409	4.1692	4	24
starved	0.5	aspartate	1.6466	0.1861	3	18

condition	time [h]	compound	concentration [mM]	SEM [mM]	campaigns	biological replicates
starved	1	aspartate	1.9927	0.2727	3	18
starved	2	aspartate	1.5059	0.1896	3	18
starved	4	aspartate	0.7701	0.0386	3	18
starved	8	aspartate	0.3238	0.0110	3	18
fumarate	ss	ATP	2.4392	0.1182	2	24
glucose	ss	ATP	1.5819	0.2577	2	24
persister	0.5	ATP	2.3893	0.2517	2	12
persister	1	ATP	2.7535	0.1602	2	12
persister	2	ATP	2.7051	0.1625	2	12
persister	4	ATP	1.7122	0.1336	2	12
persister	8	ATP	1.4283	0.4472	2	12
starved	0.5	ATP	1.9428	0.1074	2	12
starved	1	ATP	2.0406	0.1201	2	12
starved	2	ATP	1.5239	0.0800	2	12
starved	4	ATP	0.7575	0.0503	2	12
starved	8	ATP	0.3934	0.1094	2	12
fumarate	ss	cis/trans aconitate (sum)	0.0169	0.0059	2	24
glucose	ss	cis/trans aconitate (sum)	0.0060	0.0002	2	24
persister	0.5	cis/trans aconitate (sum)	0.0024	0.0005	3	18
persister	1	cis/trans aconitate (sum)	0.0021	0.0005	3	18
persister	2	cis/trans aconitate (sum)	0.0021	0.0002	3	18
persister	4	cis/trans aconitate (sum)	0.0024	0.0002	3	18
persister	8	cis/trans aconitate (sum)	0.0059	0.0007	3	18
starved	0.5	cis/trans aconitate (sum)	0.0017	0.0001	2	12
starved	1	cis/trans aconitate (sum)	0.0020	0.0006	2	11
starved	2	cis/trans aconitate (sum)	0.0024	0.0004	2	10
starved	4	cis/trans aconitate (sum)	0.0019	0.0004	2	11
starved	8	cis/trans aconitate (sum)	0.0016	0.0003	2	12
fumarate	ss	citrate	1.2367	0.4223	2	24
glucose	ss	citrate	0.5906	0.0378	2	24
persister	0.5	citrate	0.2308	0.0321	3	18
persister	1	citrate	0.1628	0.0342	3	18
persister	2	citrate	0.1966	0.0151	3	18
persister	4	citrate	0.1814	0.0112	3	18
persister	8	citrate	0.3836	0.0410	3	18
starved	0.5	citrate	0.1046	0.0035	2	12
starved	1	citrate	0.1209	0.0094	2	12
starved	2	citrate	0.0824	0.0112	2	12
starved	4	citrate	0.0661	0.0086	2	12
starved	8	citrate	0.0730	0.0069	2	12
fumarate	ss	DHAP	0.7620	0.0360	1	36
glucose	ss	DHAP	0.8272	0.0520	1	36
persister	0.5	DHAP	0.0411	0.0099	3	18
persister	1	DHAP	0.0298	0.0136	3	14
persister	2	DHAP	0.0216	0.0069	2	12
persister	4	DHAP	0.0217	0.0019	2	12
persister	8	DHAP	0.0415	0.0167	3	13
starved	0.5	DHAP	0.0481	0.0054	1	16
starved	1	DHAP	0.0478	0.0078	1	11
starved	2	DHAP	0.0106	0.0020	1	6
starved	4	DHAP	0.0108	0.0045	1	7
starved	8	DHAP	0.0057	0.0008	1	7
fumarate	ss	FAD	0.1030	0.0115	3	36

condition	time [h]	compound	concentration [mM]	SEM [mM]	campaigns	biological replicates
glucose	ss	FAD	0.0609	0.0077	3	36
persister	0.5	FAD	0.0912	0.0298	4	24
persister	1	FAD	0.1178	0.0406	4	24
persister	2	FAD	0.1332	0.0453	4	24
persister	4	FAD	0.1063	0.0357	4	24
persister	8	FAD	0.0843	0.0285	4	24
starved	0.5	FAD	0.1259	0.0454	3	18
starved	1	FAD	0.1341	0.0475	3	18
starved	2	FAD	0.1589	0.0510	3	18
starved	4	FAD	0.1073	0.0358	3	18
starved	8	FAD	0.0691	0.0240	3	18
fumarate	ss	fructose 1,6bp	0.5932	0.0531	3	36
glucose	ss	fructose 1,6bp	2.8213	0.2965	3	36
persister	0.5	fructose 1,6bp	0.0575	0.0325	3	18
persister	1	fructose 1,6bp	0.0163	0.0013	3	18
persister	2	fructose 1,6bp	0.0133	0.0033	3	16
persister	4	fructose 1,6bp	0.0161	0.0043	2	12
persister	8	fructose 1,6bp	0.0622	0.0475	3	18
starved	0.5	fructose 1,6bp	0.0171	0.0029	3	18
starved	1	fructose 1,6bp	0.0122	0.0016	3	16
starved	2	fructose 1,6bp	0.0121	0.0032	3	11
starved	4	fructose 1,6bp	0.0115	0.0035	3	7
starved	8	fructose 1,6bp	0.0084	0.0025	2	7
fumarate	ss	fructose 1p	0.0238	0.0036	2	24
glucose	ss	fructose 1p	0.0265	0.0019	2	24
persister	0.5	fructose 1p	0.0069	0.0021	3	18
persister	1	fructose 1p	0.0048	0.0016	3	18
persister	2	fructose 1p	0.0043	0.0012	3	18
persister	4	fructose 1p	0.0025	0.0008	3	18
persister	8	fructose 1p	0.0019	0.0005	3	14
starved	0.5	fructose 1p	0.0089	0.0031	2	12
starved	1	fructose 1p	0.0072	0.0018	2	12
starved	2	fructose 1p	0.0053	0.0013	2	12
starved	4	fructose 1p	0.0031	0.0006	2	12
starved	8	fructose 1p	0.0014	0.0002	2	12
fumarate	ss	fructose 6p	0.0503	0.0028	1	24
glucose	ss	fructose 6p	0.0386	0.0024	1	24
persister	0.5	fructose 6p	0.0110	0.0020	3	18
persister	1	fructose 6p	0.0077	0.0018	3	18
persister	2	fructose 6p	0.0048	0.0013	3	18
persister	4	fructose 6p	0.0027	0.0008	2	11
persister	8	fructose 6p	0.0040	0.0004	3	14
starved	0.5	fructose 6p	0.0075	0.0004	1	12
starved	1	fructose 6p	0.0051	0.0003	1	12
starved	2	fructose 6p	0.0032	NA	1	1
fumarate	ss	GDP	0.0813	0.0185	2	24
glucose	ss	GDP	0.0601	0.0047	2	24
persister	0.5	GDP	0.0734	0.0147	3	18
persister	1	GDP	0.0812	0.0256	3	18
persister	2	GDP	0.0828	0.0258	3	18
persister	4	GDP	0.0644	0.0155	3	18
persister	8	GDP	0.0410	0.0089	3	18
starved	0.5	GDP	0.1074	0.0054	2	12

condition	time [h]	compound	concentration [mM]	SEM [mM]	campaigns	biological replicates
starved	1	GDP	0.1125	0.0173	2	12
starved	2	GDP	0.1023	0.0129	2	12
starved	4	GDP	0.0780	0.0153	2	12
starved	8	GDP	0.0575	0.0235	2	12
fumarate	ss	glucose 6p	1.0688	0.0979	3	36
glucose	ss	glucose 6p	0.8133	0.1240	3	36
persister	0.5	glucose 6p	0.1707	0.0322	4	24
persister	1	glucose 6p	0.1109	0.0282	4	24
persister	2	glucose 6p	0.0559	0.0127	4	22
persister	4	glucose 6p	0.0242	0.0045	4	22
persister	8	glucose 6p	0.0446	0.0068	4	24
starved	0.5	glucose 6p	0.1410	0.0034	3	18
starved	1	glucose 6p	0.0817	0.0079	3	18
starved	2	glucose 6p	0.0222	0.0036	3	18
starved	4	glucose 6p	0.0121	0.0026	3	10
starved	8	glucose 6p	0.0070	0.0005	2	3
fumarate	ss	glutamate	19.1621	1.4438	3	36
glucose	ss	glutamate	8.7082	0.5113	3	36
persister	0.5	glutamate	10.0751	1.7600	4	24
persister	1	glutamate	7.9625	1.7807	4	24
persister	2	glutamate	8.4239	1.8612	4	24
persister	4	glutamate	17.2315	2.7883	4	24
persister	8	glutamate	26.0196	2.6968	4	24
starved	0.5	glutamate	4.5063	0.1572	3	18
starved	1	glutamate	2.6839	0.2650	3	18
starved	2	glutamate	0.8262	0.1352	3	18
starved	4	glutamate	0.6190	0.0907	3	18
starved	8	glutamate	0.8311	0.1303	3	18
fumarate	ss	GTP	0.4569	0.0752	3	36
glucose	ss	GTP	0.3758	0.0229	3	36
persister	0.5	GTP	0.2373	0.0400	4	24
persister	1	GTP	0.2517	0.0664	4	24
persister	2	GTP	0.2623	0.0657	4	24
persister	4	GTP	0.2125	0.0398	4	24
persister	8	GTP	0.1354	0.0177	4	24
starved	0.5	GTP	0.1812	0.0428	3	18
starved	1	GTP	0.1879	0.0447	3	18
starved	2	GTP	0.1343	0.0387	3	18
starved	4	GTP	0.0903	0.0253	3	18
starved	8	GTP	0.0683	0.0151	3	18
fumarate	ss	malate	19.1634	4.2980	3	36
glucose	ss	malate	1.3821	0.1962	3	36
persister	0.5	malate	0.8347	0.2423	4	24
persister	1	malate	0.9304	0.2572	4	24
persister	2	malate	1.3602	0.2625	4	24
persister	4	malate	2.9783	0.5944	4	24
persister	8	malate	13.3149	3.3080	4	24
starved	0.5	malate	0.1385	0.0398	3	18
starved	1	malate	0.1469	0.0375	3	18
starved	2	malate	0.1404	0.0284	3	18
starved	4	malate	0.0795	0.0088	3	18
starved	8	malate	0.0425	0.0098	3	18
fumarate	ss	mannose 6p	0.1919	0.0176	1	24

condition	time [h]	compound	concentration [mM]	SEM [mM]	campaigns	biological replicates
glucose	ss	mannose 6p	0.0885	0.0097	1	24
persister	0.5	mannose 6p	0.0583	0.0105	3	18
persister	1	mannose 6p	0.0400	0.0128	3	18
persister	2	mannose 6p	0.0275	0.0138	3	18
persister	4	mannose 6p	0.0153	0.0112	3	18
persister	8	mannose 6p	0.0233	0.0125	3	18
starved	0.5	mannose 6p	0.0312	0.0036	1	12
starved	1	mannose 6p	0.0174	0.0038	1	12
starved	2	mannose 6p	0.0042	0.0023	1	12
starved	4	mannose 6p	0.0062	0.0002	1	4
fumarate	ss	methylmalonate	0.4859	0.2912	2	24
glucose	ss	methylmalonate	0.0359	0.0010	2	24
persister	0.5	methylmalonate	0.0878	0.0273	2	12
persister	1	methylmalonate	0.1105	0.0108	2	12
persister	2	methylmalonate	0.1787	0.0177	2	12
persister	4	methylmalonate	0.2728	0.0756	2	12
persister	8	methylmalonate	0.4588	0.0703	2	12
starved	0.5	methylmalonate	0.0446	0.0260	2	12
starved	1	methylmalonate	0.0569	0.0199	2	11
starved	2	methylmalonate	0.0608	0.0295	2	12
starved	4	methylmalonate	0.0622	0.0273	2	12
starved	8	methylmalonate	0.0471	0.0179	2	12
fumarate	ss	NAD+	2.2482	0.3390	3	36
glucose	ss	NAD+	0.9856	0.2094	3	36
persister	0.5	NAD+	1.7407	0.6486	4	24
persister	1	NAD+	1.8783	0.6311	4	24
persister	2	NAD+	2.2058	0.7067	4	24
persister	4	NAD+	2.1157	0.7240	4	24
persister	8	NAD+	2.3151	1.0724	4	24
starved	0.5	NAD+	2.4636	0.5825	3	18
starved	1	NAD+	3.2148	1.1218	3	18
starved	2	NAD+	2.9876	0.9775	3	18
starved	4	NAD+	2.7114	0.8197	3	18
starved	8	NAD+	1.8844	0.5882	3	18
fumarate	ss	NADH	0.1481	0.0181	2	18
glucose	ss	NADH	0.0830	0.0036	2	24
persister	0.5	NADH	0.0725	0.0302	3	18
persister	1	NADH	0.1102	0.0527	3	18
persister	2	NADH	0.1398	0.0604	3	18
persister	4	NADH	0.1319	0.0553	3	18
persister	8	NADH	0.0916	0.0480	3	18
starved	0.5	NADH	0.1343	0.0201	2	9
starved	1	NADH	0.1508	0.0166	2	11
starved	2	NADH	0.1929	0.0570	2	12
starved	4	NADH	0.1706	0.0433	2	12
starved	8	NADH	0.0813	0.0042	2	12
fumarate	ss	NADP+	0.1843	0.0572	3	36
glucose	ss	NADP+	0.0942	0.0215	3	36
persister	0.5	NADP+	0.2554	0.0824	4	24
persister	1	NADP+	0.3435	0.1059	4	24
persister	2	NADP+	0.3749	0.1196	4	24
persister	4	NADP+	0.2958	0.0890	4	24
persister	8	NADP+	0.1703	0.0660	4	24

condition	time [h]	compound	concentration [mM]	SEM [mM]	campaigns	biological replicates
starved	0.5	NADP+	0.2933	0.1210	3	18
starved	1	NADP+	0.3125	0.1298	3	18
starved	2	NADP+	0.4210	0.1503	3	18
starved	4	NADP+	0.2518	0.0840	3	18
starved	8	NADP+	0.1491	0.0429	3	18
fumarate	ss	NADPH	1.7376	0.6442	2	24
glucose	ss	NADPH	0.8702	0.1488	2	24
persister	0.5	NADPH	0.3482	0.0872	3	18
persister	1	NADPH	0.8047	0.3524	3	18
persister	2	NADPH	1.6702	0.7312	3	18
persister	4	NADPH	1.2831	0.4936	3	18
persister	8	NADPH	1.3254	0.8743	3	18
starved	0.5	NADPH	1.6694	1.2796	2	12
starved	1	NADPH	1.4669	1.0938	2	12
starved	2	NADPH	1.2270	0.9007	2	12
starved	4	NADPH	0.4760	0.3301	2	12
starved	8	NADPH	0.1685	0.0800	2	8
fumarate	ss	PEP	0.6933	0.0659	3	36
glucose	ss	PEP	0.0460	0.0081	3	36
persister	0.5	PEP	2.1306	0.3543	4	24
persister	1	PEP	2.2271	0.4366	4	24
persister	2	PEP	2.2035	0.3200	4	24
persister	4	PEP	1.4215	0.2440	4	24
persister	8	PEP	1.3529	0.1908	4	24
starved	0.5	PEP	2.1943	0.5537	3	18
starved	1	PEP	2.3647	0.6946	3	18
starved	2	PEP	2.1653	0.4634	3	18
starved	4	PEP	1.1121	0.1484	3	18
starved	8	PEP	0.5296	0.0460	3	18
fumarate	ss	2-/3-phosphoglycerates (sum)	1.8921	0.1326	3	36
glucose	ss	2-/3-phosphoglycerates (sum)	0.7670	0.0747	3	36
persister	0.5	2-/3-phosphoglycerates (sum)	7.3741	1.7659	4	24
persister	1	2-/3-phosphoglycerates (sum)	7.1907	1.5898	4	24
persister	2	2-/3-phosphoglycerates (sum)	7.2862	1.2770	4	24
persister	4	2-/3-phosphoglycerates (sum)	4.7213	0.8886	4	24
persister	8	2-/3-phosphoglycerates (sum)	4.7957	0.9474	4	24
starved	0.5	2-/3-phosphoglycerates (sum)	7.4160	1.4728	3	18
starved	1	2-/3-phosphoglycerates (sum)	8.1555	1.7627	3	18
starved	2	2-/3-phosphoglycerates (sum)	6.9633	1.1611	3	18
starved	4	2-/3-phosphoglycerates (sum)	3.9816	0.3448	3	18
starved	8	2-/3-phosphoglycerates (sum)	1.9706	0.1073	3	18
fumarate	ss	phenylalanine	0.1352	0.0123	3	36
glucose	ss	phenylalanine	0.0718	0.0031	3	36
persister	0.5	phenylalanine	0.3821	0.1020	4	24
persister	1	phenylalanine	0.4193	0.0910	4	24
persister	2	phenylalanine	0.6091	0.1173	4	24
persister	4	phenylalanine	0.7210	0.3307	4	24
persister	8	phenylalanine	0.4814	0.2623	4	24
starved	0.5	phenylalanine	0.5740	0.1227	3	18
starved	1	phenylalanine	0.8724	0.1388	3	18
starved	2	phenylalanine	1.6493	0.1736	3	18
starved	4	phenylalanine	1.2183	0.1055	3	18
starved	8	phenylalanine	0.8533	0.0663	3	18

condition	time [h]	compound	concentration [mM]	SEM [mM]	campaigns	biological replicates
fumarate	ss	ribose 5p	0.2631	0.0108	1	12
glucose	ss	ribose 5p	0.4275	0.0135	1	12
persister	0.5	ribose 5p	0.0336	0.0213	2	12
persister	1	ribose 5p	0.0192	0.0120	2	12
persister	2	ribose 5p	0.0129	0.0047	2	12
persister	4	ribose 5p	0.0053	0.0010	2	12
persister	8	ribose 5p	0.0134	0.0012	2	11
starved	0.5	ribose 5p	0.0274	0.0018	1	6
starved	1	ribose 5p	0.0209	0.0011	1	6
starved	2	ribose 5p	0.0131	0.0017	1	6
starved	4	ribose 5p	0.0112	0.0013	1	4
fumarate	ss	sedoheptulose 7p	0.0539	0.0033	1	24
glucose	ss	sedoheptulose 7p	0.0726	0.0051	1	24
persister	0.5	sedoheptulose 7p	0.0278	0.0089	3	18
persister	1	sedoheptulose 7p	0.0184	0.0060	3	18
persister	2	sedoheptulose 7p	0.0079	0.0026	3	18
persister	4	sedoheptulose 7p	0.0023	0.0005	3	13
persister	8	sedoheptulose 7p	0.0031	0.0008	2	12
starved	0.5	sedoheptulose 7p	0.0209	0.0018	1	12
starved	1	sedoheptulose 7p	0.0137	0.0016	1	11
starved	2	sedoheptulose 7p	0.0079	0.0009	1	7
starved	4	sedoheptulose 7p	0.0021	0.0002	1	6
starved	8	sedoheptulose 7p	0.0019	0.0003	1	6
fumarate	ss	succinate	10.7846	2.8892	3	36
glucose	ss	succinate	0.1803	0.0169	3	36
persister	0.5	succinate	1.1454	0.1772	4	24
persister	1	succinate	1.7382	0.2620	4	24
persister	2	succinate	2.7512	0.3707	4	24
persister	4	succinate	3.8660	0.5811	4	24
persister	8	succinate	6.6663	1.4411	4	24
starved	0.5	succinate	0.0720	0.0316	3	18
starved	1	succinate	0.0621	0.0250	3	18
starved	2	succinate	0.0659	0.0265	3	18
starved	4	succinate	0.0527	0.0192	3	18
starved	8	succinate	0.0382	0.0183	3	18

Metabolite concentrations during growth on fumarate, glucose, entry into persistence and entry into starvation were measured using an LC-MS/MS method (see Experimental Procedures). Measurements were performed in 3 campaigns. In each campaign, 12 biological replicates of cells in steady state or 6 biological replicates of cells entering starvation or persistence at various time points were analyzed. Mean concentration and standard error of the mean were calculated with a mixed effects model where campaign (if data for the compound were available from different experimental campaigns) was treated as a nuisance variable. If data for the compound were available from a single campaign, mean and standard error of the mean are shown. ss – steady state.

Supplementary Table 4 – GOterms differentiating growing and persister cells, or starved and persister cells.

PCA of persister, glucose-growing and fumarate-growing cells' proteomes

GOterms characterizing growing phenotypes, based on dimension 1

Rank	GO ID	GOterm
1	GO:0009239	enterobactin biosynthetic process
2	GO:0006790	sulfur compound metabolic process
3	GO:0009432	SOS response
4	GO:0009435	NAD biosynthetic process
5	GO:0009086	methionine biosynthetic process
6	GO:0046656	folic acid biosynthetic process
7	GO:0006310	DNA recombination
8	GO:0006261	DNA-dependent DNA replication
9	GO:0042398	cellular modified amino acid biosynthetic process
10	GO:0009226	nucleotide-sugar biosynthetic process

GOterms characterizing persister phenotype, based on dimension 1

Rank	GO ID	GOterm
1	GO:0006096	glycolytic process
2	GO:0006970	response to osmotic stress
3	GO:0044260	cellular macromolecule metabolic process
4	GO:0006457	protein folding
5	GO:0042594	response to starvation
6	GO:0006006	glucose metabolic process
7	GO:0006401	RNA catabolic process
8	GO:0009063	cellular amino acid catabolic process
9	GO:0006281	DNA repair
10	GO:0009252	peptidoglycan biosynthetic process

PCA of persister, fumarate-starved and glucose-starved cells' proteomes

GOterms characterizing starved phenotypes, based on dimension 1

Rank	GO ID	GOterm
1	GO:0006099	tricarboxylic acid cycle
2	GO:0009152	purine ribonucleotide biosynthetic process
3	GO:0046129	purine ribonucleoside biosynthetic process
4	GO:0009435	NAD biosynthetic process
5	GO:0072528	pyrimidine-containing compound biosynthetic process
6	GO:0006261	DNA-dependent DNA replication
7	GO:0046487	glyoxylate metabolic process
8	GO:0015949	nucleobase-containing small molecule interconversion
9	GO:0009432	SOS response
10	GO:0006732	coenzyme metabolic process

GOterms characterizing persister phenotype, based on dimension 1

Rank	GO ID	GOterm
1	GO:0006970	response to osmotic stress
2	GO:0009252	peptidoglycan biosynthetic process
3	GO:0006412	translation
4	GO:0006096	glycolytic process
5	GO:0006401	RNA catabolic process
6	GO:0006281	DNA repair
7	GO:0006006	glucose metabolic process
8	GO:0042493	response to drug
9	GO:0044260	cellular macromolecule metabolic process
10	GO:0044267	cellular protein metabolic process

Ranked lists of 10 most enriched GOterms revealed after PCA and GOterm enrichment analyses of proteome data of persister cells, cells growing on glucose and cells growing on fumarate; as well as proteome data of persister cells, starved cells switched from glucose and starved cells switched from fumarate.

Supplementary Table 5 – Fold change in concentrations of sigma factors

	entry into persistence from glucose					entry into starvation from glucose					growth on fumarate	entry into starvation from fumarate	
gene	**0.5h**	**1h**	**2h**	**4h**	**8h**	**0.5h**	**1h**	**2h**	**4h**	**8h**		**1h**	**8h**
rpoD	1.07	1.02	1.11	1.37	1.54	1.03	1.08	1.14	1.15	1.34	0.88	1.02	1.26
rpoE	1.04	1.06	1.14	1.39	1.50	1.14	1.17	1.10	1.18	1.40	0.78	0.88	1.05
rpoN	0.86	0.86	0.86	0.87	1.00	0.94	0.87	0.90	0.86	0.85	0.99	0.89	0.90
rpoS	5.45	4.28	3.83	3.34	3.05	3.91	3.49	2.54	2.04	2.01	0.71	4.09	2.21
rpoZ	0.86	0.94	0.88	1.12	1.31	0.93	0.91	0.85	1.04	0.94	1.01	0.83	0.89

Fold change in the concentrations of sigma factors in cells during the entry into persistence and starvation, and during growth on fumarate, compared to cells growing on glucose. During entry into persistence from glucose, and entry into starvation from either glucose or fumarate, sigma factor S is more than 2-fold more abundant than during growth on glucose.

Supplementary Table 6 – Fold change in concentration of σ^S regulon proteins with more than 2-fold change at 8 hours in persister cells.

	entry into persistence					entry into starvation				
gene	**0.5h**	**1h**	**2h**	**4h**	**8h**	**0.5h**	**1h**	**2h**	**4h**	**8h**
acnA	1.11	1.45	1.96	2.86	3.29	0.96	1.15	1.29	1.45	1.53
acs	2.25	3.51	5.08	6.58	6.39	1.78	2.51	3.01	2.95	3.03
actP	1.82	2.75	3.68	4.87	5.29	1.42	1.99	2.14	1.83	1.73
aidB	0.96	1.72	3.48	6.03	6.95	1.73	1.76	2.74	3.14	3.32
aldB	2.80	5.24	10.08	17.15	26.34	2.27	4.36	5.47	6.24	7.04
araF	2.89	4.26	6.36	14.12	19.20	2.16	3.66	6.27	6.74	8.56
araG	0.23	0.56	2.05	2.78	11.08	0.37	0.21	2.25	1.22	3.53
astA	1.56	3.71	6.97	13.84	13.70	1.81	2.82	5.67	5.64	6.73
astB	0.38	0.68	1.76	2.67	2.37	0.48	0.43	1.08	0.87	0.83
astC	2.05	3.51	5.82	8.07	5.48	2.11	3.16	4.47	4.83	4.56
astD	1.66	1.97	3.51	7.01	4.96	1.77	2.14	2.42	3.49	4.64
astE	0.81	5.86	14.61	44.08	42.93	1.54	4.88	12.85	13.67	8.03
bolA	3.13	4.03	5.49	4.52	4.18	3.17	3.96	4.74	4.66	3.47
cbpA	0.94	1.16	1.29	1.75	2.09	0.87	0.88	0.96	1.12	1.17
cfa	0.17	0.14	0.08	0.13	0.20	0.11	0.03	0.00	0.01	0.01
csiD	18.01	16.75	12.98	12.89	15.03	17.68	19.31	18.96	9.07	8.19
csiE	4.56	9.22	17.30	18.46	20.04	3.69	6.66	9.11	7.65	8.71
ddpA	1.11	1.42	1.57	2.60	3.22	1.16	1.30	1.23	1.28	1.11
dps	1.01	1.43	2.17	1.98	2.45	0.89	1.59	2.17	2.16	2.32
ecnB	1.42	1.98	2.61	4.16	5.71	1.32	1.60	2.06	2.16	2.34
fadL	25.56	30.61	58.85	36.89	19.40	19.99	15.70	10.74	7.26	6.66
fic	1.35	2.03	2.44	3.75	4.82	1.38	1.74	2.05	2.28	2.66
frdA	1.64	1.82	2.88	3.78	4.54	1.13	1.41	1.80	1.45	1.53
frdB	1.95	2.39	3.05	4.04	4.57	1.29	1.38	1.30	1.53	1.78
ftsB	0.88	0.89	0.70	0.56	0.37	1.05	0.79	0.58	0.45	0.27
gadA	0.25	0.60	1.60	4.44	18.24	0.30	0.25	0.90	1.48	1.86
gadB	1.10	1.49	2.13	5.78	13.51	1.09	1.11	1.58	2.07	1.28
glgS	4.74	11.69	24.69	36.15	48.07	5.77	9.84	14.77	27.57	25.35

	entry into persistence					entry into starvation				
gene	**0.5h**	**1h**	**2h**	**4h**	**8h**	**0.5h**	**1h**	**2h**	**4h**	**8h**
gmr	4.73	4.44	8.02	9.59	4.81	3.35	5.00	5.50	1.91	1.70
hchA	1.59	2.59	5.21	7.60	11.70	1.37	1.88	2.96	2.84	3.51
hdeA	0.56	0.67	0.78	2.41	5.48	0.39	0.45	0.60	0.76	0.81
hdeB	0.61	0.80	0.99	4.55	9.92	0.41	0.46	0.82	0.97	1.16
hmp	1.03	0.92	0.83	0.35	0.36	1.08	0.99	0.83	0.70	0.58
ihfA	1.20	1.38	1.62	2.08	2.31	1.14	1.47	1.29	1.25	1.33
ihfB	1.22	1.33	1.50	2.10	2.37	1.23	1.27	1.32	1.30	1.53
katE	0.37	0.27	0.17	0.12	0.16	0.30	0.24	0.16	0.10	0.11
ldcC	1.56	1.60	2.14	2.61	3.29	0.94	1.15	1.36	1.53	2.19
lhgO	1.37	1.96	1.90	2.20	3.78	1.34	1.64	1.73	2.01	2.34
lsrA	1.05	2.60	2.95	2.74	3.74	1.54	1.97	1.36	1.58	2.08
lsrB	1.60	5.07	5.02	7.41	9.05	1.24	2.91	3.70	4.37	3.98
lsrF	1.49	4.28	5.45	6.06	5.69	1.29	2.87	4.02	3.65	2.71
lsrG	2.28	5.75	5.53	4.95	7.90	1.29	3.58	4.76	3.05	2.99
mdtA	1.63	1.80	2.09	2.40	2.19	1.62	1.95	1.50	1.92	2.32
mglA	1.42	1.54	2.04	2.16	2.42	1.52	1.61	1.80	1.57	1.62
mglC	3.03	3.23	3.50	4.10	7.79	2.99	3.27	4.24	3.08	3.21
msyB	1.26	1.84	2.24	3.80	4.91	1.22	1.30	1.63	1.84	1.96
osmB	1.25	2.77	4.67	8.22	8.42	1.35	2.33	2.88	4.32	3.40
osmC	1.45	1.71	1.77	2.69	3.57	1.66	1.63	1.78	1.86	2.01
osmE	1.30	1.65	2.02	2.94	3.46	1.07	1.16	1.36	1.33	1.40
osmY	1.17	1.13	0.83	1.91	2.86	1.06	0.95	1.24	1.02	0.94
otsA	1.06	1.19	1.37	1.61	2.57	0.96	1.06	1.04	0.96	1.17
poxB	1.03	1.18	1.43	1.78	2.34	0.98	0.98	1.12	1.11	1.15
puuA	0.41	0.25	0.09	0.09	0.15	0.39	0.30	0.05	0.20	0.22
puuB	0.13	0.05	0.02	0.06	0.05	0.09	0.14	0.05	0.03	0.04
puuC	0.57	0.51	0.34	0.15	0.11	0.59	0.49	0.34	0.21	0.18
puuD	0.90	0.92	0.86	0.66	0.18	0.70	0.69	0.49	0.33	0.16
puuE	0.57	0.51	0.31	0.10	0.07	0.48	0.39	0.30	0.20	0.18
rsd	1.14	1.06	1.12	0.54	0.45	1.15	1.23	0.84	0.63	0.67
sodC	1.56	1.84	1.36	5.54	10.84	1.56	1.24	1.95	2.27	2.33
sra	0.98	1.07	1.27	2.18	2.06	1.03	1.15	1.48	1.01	1.26
talA	1.08	1.25	1.43	1.91	2.24	1.20	1.15	1.25	1.40	1.43
tam	0.87	1.02	3.18	5.63	8.63	1.42	2.02	2.52	2.03	3.19

	entry into persistence					entry into starvation				
gene	**0.5h**	**1h**	**2h**	**4h**	**8h**	**0.5h**	**1h**	**2h**	**4h**	**8h**
tktB	1.03	1.13	1.28	1.57	2.01	1.04	1.08	1.20	1.16	1.20
treA	1.43	2.00	2.40	2.88	2.90	1.37	1.45	1.68	1.62	1.46
uspB	6.88	6.29	6.99	5.62	4.39	6.84	7.64	6.36	4.54	3.66
wrbA	1.02	1.14	1.44	1.84	2.18	0.97	1.05	1.25	1.29	1.39
ybjP	1.14	1.52	2.02	2.91	3.69	1.02	1.18	1.45	1.46	1.60
yccJ	1.30	1.62	2.31	4.28	6.36	1.23	1.51	1.86	2.03	2.28
yciE	1.01	1.07	1.27	1.46	2.97	1.08	1.10	1.41	1.34	1.09
yciF	1.47	1.60	2.54	5.53	10.13	1.51	1.55	1.60	1.33	0.80
yciG	4.63	77.65	6.38	425.50	525.30	11.18	11.50	14.59	8.43	35.21
ydcS	2.86	5.16	5.94	8.70	9.24	2.18	2.97	3.19	2.80	2.97
ydcT	19.04	29.47	57.32	77.49	75.01	11.47	27.76	31.02	25.81	26.65
yegQ	0.90	0.84	0.65	0.40	0.25	0.92	0.87	0.68	0.61	0.49
yegS	0.65	0.84	1.60	2.23	3.43	0.90	1.09	1.03	1.19	1.37
ygaU	1.60	1.80	2.56	3.78	6.22	1.40	1.65	1.85	1.75	1.95
yhjG	1.31	1.62	1.25	1.49	2.10	1.91	0.82	0.78	1.87	1.43
yjcH	7.82	10.70	17.22	22.24	24.90	4.15	7.31	9.49	6.16	6.72

Fold-change in concentrations of proteins regulated by σ^S in cells during the entry into persistence and starvation, compared to cells growing on glucose. Almost half of the proteins regulated by σ^S are more than 2-fold up- or down- regulated during the entry into persistence.

Supplementary Table 7 – Change in antibiotic tolerance to ampicillin after nutrient-shift in mutant strains.

Strain	Fraction of antibiotic-tolerant cells in the mutant strain	Fraction of antibiotic-tolerant cells in the respective WT background	Change in fraction of the antibiotic-tolerant cells compared to the respective WT (±SD)	p-value (t-test)
MG1655 Δ10	0.953 ± 0.016	0.963 ± 0.023	-0.01 ± 0.027	0.26
MG1655 Δ10ΔrpoS	0.695 ± 0.033		**-0.268** ± 0.04	**0.001**
BW25113 Δrmf	0.960 ± 0.016	0.955 ± 0.009	+0.005 ± 0.018	0.6
BW25113 ΔrelA	0.954 ± 0.011		-0.001 ± 0.015	0.88
BW25113 ΔrpoS	0.571 ± 0.069		**-0.384** ± 0.07	**<0.001**

Supplementary Table 8 – Primers used for TAS transcript quantification

Gene name	Classification	Forward primer	Reverse primer
mazE	TAS-AT	ATGATCCACAGTAGCGTAAAGCGT	ATTGAGCGCCTGCATTAACGTA
chpS	TAS-AT	TGCTGGCACAGTGTGACATG	GGGTGGATTTACCCCAGACA
hicA	TAS-T	TGGGAGGCGCAGTGTCA	TTTACGCAATGGTTCTTTAATCTCA
mqsR	TAS-T	CGCACACCACATACACGTTTG	ACTTGCCCGGCATTGACA
rnlA	TAS-T	GCTCGTTTCAGGGCTATGTGTT	AATGGTGCGTAGTTCAGGATAAAGT
relB	TAS-AT	GACGATGAACTTAAAGCGCGTT	GAAGGAGTTACACCCATTTTTTCAAG
yefM	TAS-AT	CGCTGGAAGAGACGGCTTAT	AGGCTATCGATTGAGTCCATCAA
yafN	TAS-AT	AACAAGAGGAGAAAAAGCCCATAA	GCGTGTAATTTCCTCTAATCTTGCA
dinJ	TAS-AT	AGAATCAGGCAGCGGACGTA	TGCGAACCAGGTCAGAGATG
higB	TAS-T	GCATTGAAAGATGCTGCGGA	CCAGAGCCACCAACTCCGTT
ratA	TAS-T	GTTGTACCGGAAGTCGGATTCT	TGATCCCAGCCTTAGAGACATCTA
hipB	TAS-AT	TGGGAGGCGCAGTGTCA	TTTACGCAATGGTTCTTTAATCTCA
yjhX	TAS-T	GTCAGGAACAACATACCTTACACGTT	AGTGACGCGGCCTGAAGA
argE	Housekeeping	CGATACGGTGCCATTTGATG	TCATGCTCCGTCAGTGTAAACG
rhlB	Housekeeping	CGTGGCGATCTGGATATTCTG	TGCCGGAATATGCAAACCA
panC	Housekeeping	CCTGCTTCGGTGAAAAAGATTT	GCCCATATCGGCAACCATT
tufA	Housekeeping	CACCCCGACCCGTCACTAC	CACCGGTGATCATGTTTTTAACA
rplA	Housekeeping	ACTGTACTGCCGCACGGTACT	GCGTTTGCACCTTGGGTAA
gapA	Housekeeping	GCTCAGAAACGTTCTGACATCGA	CAGCATGTATGCCATGTAATCAG

Supplementary Table 9 – Settings of STEM software

Section	Setting	Value
Main Window	No normalization/add 0	checked
Main window	Gene Annotation Source	Escherichia coli (EcoCyc & EcoliHub)
Main window	Clustering Method	STEM Clustering Method
Main window	Maximum Number of Model Profiles	30
Main window	Maximum unit Change in Model Profiles between Time Points	2
Filtering	Maximum Number of Missing Values	0
Filtering	Minimum Correlation between Repeats:	0
Filtering	Minimum Absolute Expression Change	1
Filtering	Change should be based on	Difference from 0
Filtering	Pre-filtered Gene File	<empty>
Model Profiles	Maximum Correlation	1
Model Profiles	Maximum Number of Candidate Model Profiles	1000000
Model Profiles	Number of Permutations per Gene	0 (all permutations)
Model Profiles	Significance Level	0.05
Model Profiles	Permutation Test Should Permute Time Point 0	Unchecked
Model Profiles	Correction Method	False Discovery Rate
Clustering Profiles	Minimum Correlation	0.6
Clustering Profiles	Minimum Correlation Percentile (repeat only)	0

Unspecified settings were left at default values. Short Time-series Expression Miner (STEM) version 1.3.8 was used for analysis.

Supplementary Texts

Supplementary Text S1: Evaluation of the effects of the presence of non-persister cells on the determined persister phenotype

In this text, we demonstrate that the small fraction of growing cells occurring after a glucose to fumarate shift does not significantly influence the reported values describing the phenotype of persister cells. For this analysis, we used two datasets: (i) a dataset describing cells growing normally on fumarate and (ii) a dataset describing the mixed population obtained after a glucose to fumarate shift (i.e. containing mostly persisters, and some cells growing on fumarate). We also used the information about the actual fractions of cells growing on fumarate in this mixed population. These datasets allowed us to determine the effect that the cells growing normally on fumarate would have on the reported measurements from the mixed population.

Worst-case scenario

After a switch from M9-glucose to M9-fumarate medium a small fraction of cells adapt to the new growth medium, while the rest adopt a non-/slow-growing, antibiotic-tolerant phenotype (Kotte et al., 2014). In the current paper, we confirm this finding in

Supplementary Figure 1A. From the cell population used to inoculate the new growth medium, only 0.1 ± 0.05% (SD) of cells adapt to grow on fumarate. 10-15 hours after the switch, the growing population reaches 1% of total population (Supplementary Figure 1A). Because of the inherent difficulty in measuring small fractions of cells, we can only estimate how many growing cells are present at 8 hours after the switch, which is the time point until which we characterized the persister cells. To do a worst-case estimation of the effect of growing cells on the determined persister phenotype, we assumed that 1% of normally growing cells is already reached 8 hours after the switch. For the estimation of the effect of the presence of the growing cells, we further assumed that the growing cells have already reached their new steady state 8 hours after the switch (which is also a conservative estimate).

Formula for calculating the effect of growing cells on results of persister cells

If our population is a mixture of two populations, every quantified value will be result of a weighted average. In our particular case, each value can be expressed as $X = aY + bZ$, where Y is the true value for persister cells and Z is the true value for growing cells, a is the fraction of persister cells and b is the fraction of growing cells. Consequently, we can calculate the true value for slow-growing cells: $Y = (X - bZ) / a$. We will use this above formula in the following to show that the influence of growing population does not elicit a

statistically significant difference. We propagated errors according to $\Delta Y = \sqrt{(\Delta X^2+(b\Delta Z)^2))}/a$.

Growing population does not influence the physiological data

Physiological rates of persisters were de-convoluted using the formulas described above, the measured physiological rates of mixed populations and the measured physiological rates of fumarate-adapted cells (Supplementary Figures S1B and S1C). Here, we found that the 95% confidence interval of the mean values of calculated rates overlap between the mixed-population and de-convoluted values in the worst-case scenario.

Growing population does not influence the metabolite concentration measurements

Metabolite concentrations were de-convoluted as described above. For all measured metabolites, the 95% confidence interval of the mean values of metabolite concentrations overlapped between concentrations we report and the de-convoluted concentration (Supplementary Figure 1D). Thus, the possible difference elicited by growing cells in this worst-case-scenario is smaller than the accuracy of the method.

Growing population does not influence the protein concentration measurements

Also for the proteome data, we applied the same deconvolution method. Then, we compared correlation coefficients of the mixed population proteome and the de-convoluted proteome to detect differences between proteomes. We found that their Pearson's r equals 0.99998. The average Pearson's r between three biological replicate measurements of glucose-growing cells' proteomes is equal to 0.989. Thus, the possible difference elicited by the small fraction of growing cells even in the worst-case-scenario is smaller than the accuracy of the method and thus negligible.

Concluding remarks

Together, even considering a worst-case-scenario (assuming that at 8 hours already 1% of cells belong to the growing phenotype), the small fraction of growing cells does not affect the values that we report for the persister cells in a significant manner.

Supplementary Reference List

Keseler, I.M., Mackie, A., Peralta-Gil, M., Santos-Zavaleta, A., Gama-Castro, S., Bonavides-Martinez, C., Fulcher, C., Huerta, A.M., Kothari, A., Krummenacker, M., *et al.* (2013). EcoCyc: fusing model organism databases with systems biology. Nucleic Acids Res. *41,* D605-D612.

Kotte, O., Volkmer, B., Radzikowski, J.L., and Heinemann, M. (2014). Phenotypic bistability in Escherichia coli's central carbon metabolism. Molecular Systems Biology *10,* 736.